ABSTRACT

Title of Document:	MODELING OF A HIGH ENERGY DENSITY PROPULSION SYSTEM BASED ON THE COMBUSTION OF ALUMINUM AND STEAM.
	Walter Ethan Eagle, Master of Science, 2007
Directed By:	Associate Professor Christopher P. Cadou, Aerospace Engineering Department

This thesis presents a thermodynamic analysis of a novel Rankine cycle aluminum/steam combustion power system being developed for use in Unmanned Underwater Vehicles (UUVs). The analysis is performed using a system modeling tool developed by the NASA Glenn Research Center called Numerical Propulsion System Solver (NPSS). Thermodynamic models of the individual components are created and linked together in NPSS, which then solves the system by enforcing mass and energy conservation. Design and off-design conditions are simulated and predicted performance is compared with predictions made by two other research groups. The simulations predict that this power system could provide at least five-fold increases in range and endurance for the US Navy's 'Sea Horse' UUV. A rudimentary sensitivity analysis is used to identify the factors which most strongly influence the performance of the design. Lastly, recommendations for future work and possible model improvements are discussed.

MODELING OF A HIGH ENERGY DENSITY COMBUSTION BASED ALUMINUM
AND STEAM PROPULSION SYSTEM.

By

Walter Ethan Eagle

Thesis submitted to the Faculty of the Graduate School of the
University of Maryland, College Park, in partial fulfillment
of the requirements for the degree of
Master of Science
2007

Advisory Committee:
Associate Professor Christopher Cadou, Chair
Associate Professor Kenneth Yu
Associate Professor Robert Sanner

Dedication

To my family and friends, without whom none of this would have been possible.

Acknowledgements

Table of Contents

List of Figures

List of Tables

Chapter 1: Introduction

1.1 *Motivation for Chemical / Thermal Propulsion*

Figure 1.1 US NAVY 'Sea Horse' Developed by ARL

The range and endurance of unmanned underwater vehicles (UUVs) like the US Navy's 'Sea Horse' is limited by the energy density and overall thermodynamic efficiency of their power systems [1]. This can be seen using a simple analysis analogous to that used to develop the Breguet range equation for aircraft [2]: The range of an underwater vehicle is determined by its cruise velocity and the time its propulsion system operates.

$$R = \int_{0}^{t_{run}} v_c dt \qquad\qquad (1.1.1)$$

Neglecting the work associated with changes in cruise depth, the total energy expended during the mission equals that used to overcome drag. This is given by:

$$E_D = \int_0^{t_{run}} F_D v_c \, dt \qquad\qquad (1.1.2)$$

Equating the total energy expended during the mission to the total energy stored on board the vehicle times an overall efficiency, and assuming that the mission is performed at constant velocity leads to:

$$F_{thrust} v_c t_{run} = V_{prop} Q_V \eta_{net} \qquad\qquad (1.1.3)$$

The thrust can be expressed in terms of a drag coefficient:

$$F_{thrust} = \frac{1}{2} C_D v_c^2 A \qquad\qquad (1.1.4)$$

Solving 1.1.2 for $v_c t_{run}$, and substituting this into Eqn.1, again assuming constant cruise speed, gives the following expression for the vehicle's range:

$$R = v_c t_{run} = \frac{V_{prop} Q_V \eta_{net}}{F_{thrust}} = \frac{2V_{prop} Q_V \eta_{net}}{C_D v_c^2 A} \qquad\qquad (1.1.5)$$

Equation 1.1.5 shows that the range is determined by the vehicle size (A, C_D), the cruise speed (v_c), the volume of the propellant (V_{prop}) stored aboard the vehicle, the volumetric energy density of the propellant (Q_V [W-hr/L]), and the overall conversion efficiency of the power system (η_{net}). Equation 1.1.5 is used to generate figure 1 which shows contours of range for a typical UUV (10,000lb) fielded by the US Navy called the 'Sea Horse'.
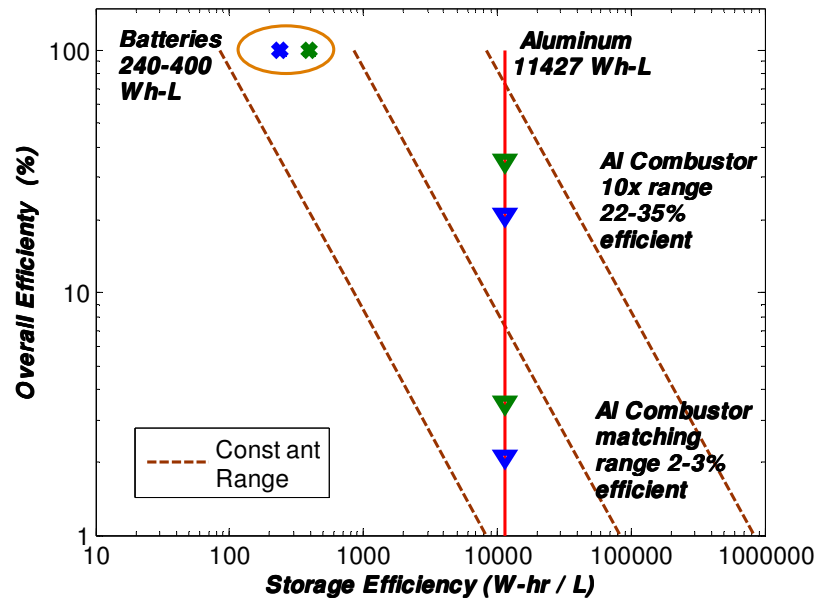
Figure 1.2 Range as a function of fuel storage efficiency and overall system efficiency. Calculation based on current projections of velocity, power consumption, and storage for propellant.

The dotted lines in figure 1 show contours of constant range. The vertical line in figure 1 corresponds to the energy density of Aluminum which is approximately 30-50 times greater than the batteries presently available for use in the Sea Horse. Hence, a propulsion system based on the exothermic reaction of aluminum with sea water has tremendous potential for increasing the Sea Horse's range and endurance. However, the figure also shows that this energy density advantage will not be realized unless the energy system is able to operate efficiently. The blue and green symbols refer to two different types of batteries that could be used to power this vehicle. The lower pair of triangular symbols indicate the level of thermodynamic energy conversion efficiency required of the Aluminum combustion system to match the ranges of the competing battery systems (low and high storage efficiency). The upper pair of triangular symbols shows the efficiency required to achieve a tenfold increase in range. These symbols show that an overall

3

thermodynamic efficiency of only 2-3 % is required in order to match the performance of the current system and an efficiency of 22-35 % is required to improve range by an order of magnitude.

The principal objective of this thesis is to establish the level of overall thermodynamic efficiency that can reasonably be expected from an aluminum/sea water propulsion system so that the viability of the concept can be determined. This will be accomplished by developing a detailed thermodynamic model for a prototype aluminum combustion propulsion system being developed for the Sea Horse by Penn State's Advanced Research Laboratory. The ARL propulsion system, the modeling approach, and the thesis objectives are described in more detail below.

1.2 *Combustion of Aluminum*

1.2.1 Balanced chemical reaction

The oxidation of aluminum particles was first characterized in O_2 in the late 1940s and early 1960s [3-7]. The balanced chemical reaction is given by:

$$Al(s) + 3/2 O_2(g) \rightarrow Al_2O_3(s) \quad \Delta H = -1.6 \, MJ/mole \quad (1.2.1)$$
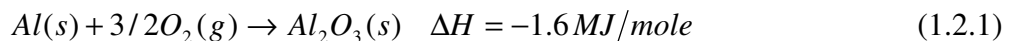
The balanced chemical reaction for aluminum with steam is given by:

$$2Al(s) + 3H_2O(g) \rightarrow Al_2O_3(s) + 3H_2 \quad \Delta H = -962 kJ/mole \quad (1.2.2)$$

The heat of combustion of aluminum in steam is 17.87 kJ/g and the adiabatic flame temperature at one atmosphere is 3036K. This high temperature is characteristic of metal combustion and is lower than the adiabatic temperature in O_2 which is 4005K. These predictions are calculated using CEA, the NASA chemical equilibrium program at 1atm

and 298K reactants[8]. While less energy is liberated in the Al-H$_2$O reaction, ignition temperatures for Al particles in H$_2$O are observed to be almost 600K lower than in O$_2$ [7]. They attribute this phenomenon to the presence of a hydroxide coating (Al-OH) that is less protective than the oxide coating (Al$_2$O$_3$) present in air.

1.2.2   Aluminum particle combustion process

Aluminum is usually stored in the form of particles because these particles have high surface-to-volume ratios and are easily entrained in streams of gaseous oxidizers. Particles nominally range in size from 10s of nanometers to 10s of microns and are all covered with a thin (20 nm) oxide layer [9]. This layer is inert and must be cracked in order to initiate reaction with the Aluminum core. Figure 3 is a photograph of an aluminum particle roughly 50 microns in size burning in air at 1 atm. The high temperature of the mixture of combustion products and air surrounding the particle vaporizes the solid aluminum core and this vapor escapes producing a diffusion flame around the molten Al droplet [5]. This diffusion controlled combustion has been characterized by several studies of single particles burning in O$_2$ [3,4,6,7,10], air [5, 11-15], and CO$_2$ [16,17] and finally in computational models [18-20].

Figure 1.3 Diffusion controlled burning of large (micron) aluminum particles in air. Ref. [5]
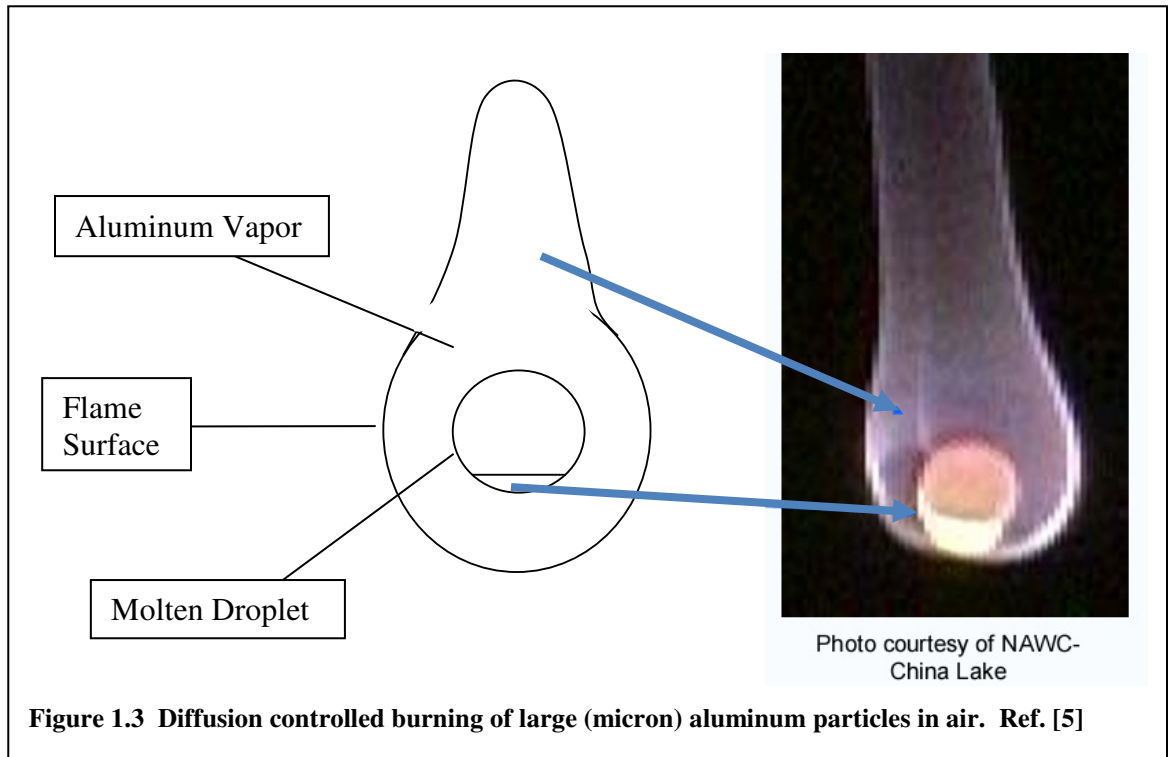
However, in the reaction of interest, Al/H$_2$O at high pressure, there is evidence to support

the idea that aluminum particle combustion occurs at the surface [21]. The reason for this

is straight forward: with steam at pressures greater than 5 atm, the vaporization

temperature of Al actually exceeds the predicted adiabatic flame temperature [8]. Under

these conditions, the combustion process does not generate enough heat to vaporize the

aluminum and the reaction must occur on the particle surface. This is problematic

because the vaporization temperature of aluminum oxide is even greater than the

aluminum.   This means that the aluminum oxide condenses on the particle surface

thereby increasing the thickness of the passivating oxide layer. As a result, the reaction

rate depends on the rate at which the oxidizing layer cracks open, exposing molten

aluminum[21].

1.2.3 Dust Cloud Combustion

While most investigations of aluminum combustion have focused on single particles, in practical systems it is actually a cloud of aluminum particles that is burning. Experimental studies of this process have been undertaken for Al O_2/N_2 and Al H_2O systems [9,10,15,22-25]. In the variety of conditions examined by Goroshin et al. [10], the flame speed of aluminum aerosols was constant in oxygen rich environments as dust concentration was varied. However, the flame speed showed a strong dependence on the initial temperature of the cloud. Creating theoretical models for this type of combustion is extremely difficult because contributions from particle interactions, various modes of heat transfer, flame structures and aerosol gas thermal properties all affect the reaction progress.

1.2.4 Considerations for Nano-Al Particles

The work of Yetter and Yang in the area of aluminum combustion has focused on a mix of nano and micro-sized aluminum particles in varying oxidizers including water with the intent of advancing the application to underwater propulsion technologies [9,22-27]. The primary interest in nano-particle mixtures is the enhancement in overall energy density due to increased particle packing density.

Another potential advantage of nano-scale particles is enhanced reactivity leading to lower ignition temperatures and shorter reaction times. Theoretically speaking, as the particle size begins to drop, the reaction should transition from a diffusion-limited to a kinetically-limited regime. The work of Krier, Glumac and Bazyn and Risha, Yetter, and Yang, simultaneously has begun to experimentally validate this by showing that combustion temperature, reaction rate, and sensitivity to pressure scale differently with

particle size depending on whether the particles are micro or nano-sized. [22-24]. They illustrated that nano-particle ignition temperatures are as low as 1200K at 1atm; more than a 700K drop from the roughly 2000K ignition temps reported for micron size particles. They go on to explain that as the particle diameter shrinks, heat transfer due to convection and radiation also become more significant and particles can heat up. Higher particle temperature significantly affects the reaction rate with Arrhenius-type exponentials fitting nano-Al combustion data [22]. For very small nano-particles, the surface-to-volume ratio may be so large that the surface energy becomes dominant leading to properties (melting/boiling points) that differ from "bulk" properties of Al [24].

The small scales of these particles lead to extremely small characteristic times for mass and energy transport. Risha et al. describe this process in terms of the Knudsen number (Kn), the ratio of mean free path to the particle radius, which for nano-scale flows is near unity [9]. Since the mean free path depends on the density or pressure, combustion processes will no longer be independent of pressure as they are in gas-diffusion limited combustion regimes.

There is however a probable limit where reducing the particle size is no longer beneficial. Analysis of pre and post combustion products in Risha et. al's study also predicts that the oxide layer thickness on the unreacted particles is on the order of 20nm [9]. This estimate is an important measurement, for as particle size shrinks, the proportion of aluminum oxide to aluminum (and hence the energy density of the particle) follows the surface-to-volume ratio of the particle and begins to decrease dramatically. Hence there is first a rise

in energy density as particle size drops, but then a sharp fall. This indicates that an optimum particle size exists.

1.2.5 Engineering challenges

The critical engineering issues associated with building practical Aluminum combustors are summarized by Foote et al.[28] who also investigated the effects of combustor heat transfer, ignition requirements, and residence times. One important consideration noted in this study is 'slagging,' which refers to the tendency of the Al_2O_3 in the combustion products to condense and agglomerate to form large solid particles. Slag can adhere to the combustor/nozzle walls, clogging the flow passages and hindering performance[18]. The large particles are a threat to moving components and must be removed from the gas flow in closed cycle engines before it enters the turbine or other components with moving parts. Therefore, any practical system must be designed with these considerations in mind.

1.3 *Aluminum Fuel for Underwater Vehicles*

Although it was recognized that metal fuels could be utilized as a new power source for underwater vehicles, it was not until the 1960's that it was proposed that energy could be stored in metals that react exothermically with water like Al, Zr, Mg, and Li [29]. Vehicle range would be improved because one reactant, in this case water, could be harvested from the environment in the same way that aircraft engines harvest oxygen from the air. This could increase the range of a high speed torpedo by a factor of four [29]. This work was theoretical, however, and many of the experimental problems of aluminum

combustion like the difficulty in initiating and sustaining the combustion reaction were left unaddressed.

Beginning in the 1970's several studies appeared discussing the practicality of storing fluidized powdered fuels for rocket applications [30]. By this time, Aluminum had been identified as a usable propellant additive to mitigate combustion instability problems in solid rocket boosters and as a way to increase energy density [31]. Aluminum was also considered as a primary propellant option since its products are completely benign [32,33]. Through investigating the role of aluminum on combustion instability, it was discovered that Al/H_2O was the primary contributor to the reaction in solid state rockets, and it was noted that this reaction liberated even more H_2[33]. With this as impetus, the Aluminum/Water combustion was studied extensively and its detailed chemical evolution was described [34].

In the 1980's researchers again began to study metal reactions for underwater closed cycle propulsion systems [35]. Again, Aluminum was again identified as a possible fuel and a design for exploiting it was described by Kiely [36]. Table 1.1 shows that the aluminum water reaction offers the highest volumetric energy density (11500 W-hr/L) compared to other propellant options [1]. While some reactions have higher specific energies than Al/H_2O, their higher cost and the toxicity of the metals make them undesirable choices [32].

Fuel	Oxidizer	Specific Energy W-hr/kg	Energy Density W-hr/L
Al	H_2O	4200	11427
Zr	H_2O	1575	10264
Al	$LiClO_4$	3478	8821
Mg	H_2O	3733	6876
Li	H_2O	7408	3970
Otto fuel		705	895
Batteries		100-150	240-389

Table 1.1 Fuel Energy Density for a variety of metals, compared to traditional monopropellant and batteries.

Furthermore, unlike aircraft applications where weight is the primary concern (i.e. where Li-H_2O would be favorable over Al-H_2O), volume is the primary concern under water since no induced drag occurs underwater because the vehicles are neutrally buoyant. For this reason the Al-H_2O system is preferred for underwater applications. Table 1.1 shows that a combustion powered system would only need to achieve an overall energy conversion efficiency of 4% to match the range of the battery powered system.

As modern torpedo borne Rankine cycle steam turbines achieve efficiencies of up to 30%, interest burgeoned in applying the aluminum water reaction in an underwater thermal propulsion system [36]. Starting in 2002, the Penn State Advanced Research Lab (ARL) began conducting research with the support of the Naval Underwater Warfare Center (NUWC), Defense Advanced Research Project Agency (DARPA) and the Office of Naval Research (ONR) in the development of an underwater propulsion system based on combustion of powdered aluminum with seawater [1]. This work addressed problems with particle injection encountered in older model vortex combustors and demonstrated

steady state combustion of aluminum and water albeit over relatively limited operating times (10 to 90 minutes). The key practical challenges remaining include ignition concepts at the vehicle level, flame stabilization over a dynamic range of operating conditions, overall efficiencies over said range, and most notably, slag formation and its effects on system reliability or maintainability.

1.4   *Objectives and Approach*

The objective of this thesis is to estimate the power output and overall efficiency of the Rankine Cycle propulsion system outlined in Figure 1.4. It is based on the exothermic reaction of aluminum powder with sea water and a prototype of the system is presently being constructed by ARL for DARPA. The prototype is intended for use in small (10,000lb) Unmanned Underwater Vehicles (UUVs) like the Sea Horse.
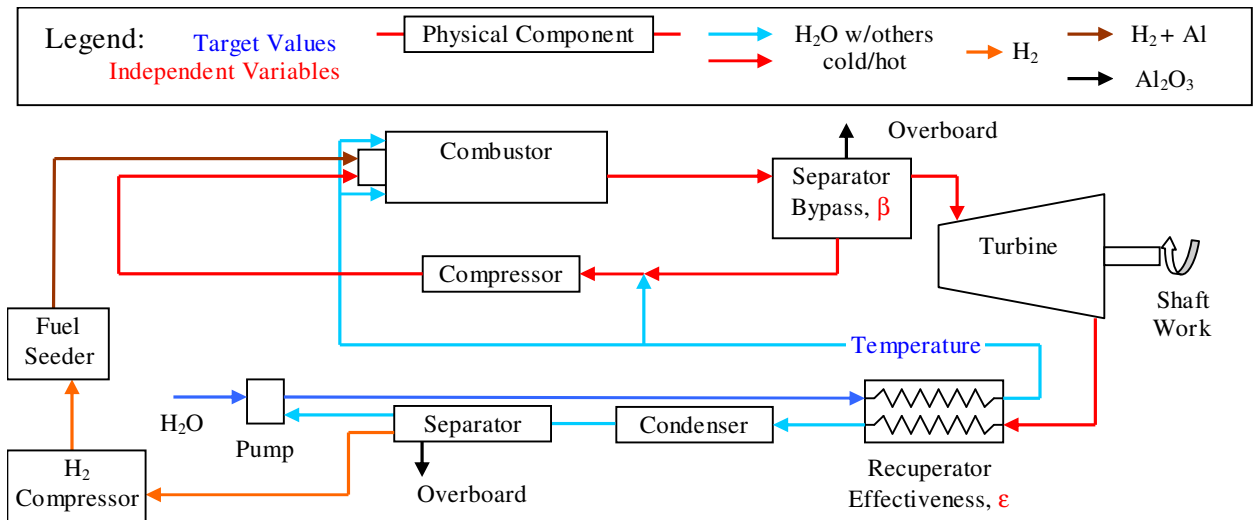
Figure 1.4 System Schematic

The basic operation of the system is as follows: Aluminum powder is suspended in a small flow of gaseous hydrogen and transported to a combustor where it reacts

exothermically with steam to form $Al_2O_3(s)$ and H_2. Additional water injected into the reacting flow cools the hot products, producing steam. The combustion products pass through a separator to remove the solid Al_2O_3. Most of the steam hydrogen mix is then passed to a turbine that drives an alternator. A small fraction of the steam/hydrogen is diverted from the separator, cooled to 900F by a small amount of fresh sea water, compressed, and returned to the entrance of the combustor to sustain the reaction with incoming Aluminum powder. Enthalpy remaining in the flow exiting the turbine is recovered using a heat exchanger and pre-heats the combustor cooling water. The steam is finally condensed and separated from the H_2. The water is recycled through a pump which draws in an appropriate amount of fresh water to make up for that spend during combustion. The hydrogen gas is compressed and fed back into the fuel feeder, thus completing the cycle.

The approach taken to estimate the system's performance is to develop thermodynamic models for each individual component in the system, and then to assemble the individual models to create a model of the entire system. This is accomplished using a specialized software package called Numerical Propulsion System Solver (NPSS) [37], which was originally developed by the NASA Glenn Research Center as a generalized design and analysis tool for developing gas turbine engines although it is equally well-suited for Rankine Cycle analyses. The principal advantage of NPSS is that it takes care of the mathematical difficulties associated with solving systems of interacting thermodynamic components, enabling the focus to be placed on developing appropriate component models. NPSS creates generalized data structures for passing information between components and implements a Newton-Rhapson solver to find stable operating points.

Other important advantages of NPSS are its graphical user interface with extensive libraries of pre-defined components, the ability to develop new components and add them to the library, and a very high degree of flexibility in the types of component models that it can accept. For example, a turbine could be modeled in NPSS either by writing a module in C that incorporates the simple governing equations found in a textbook (with overall efficiency as a parameter), by using a multi-dimensional turbine map, or by linking to an external 3D CFD simulation. It also facilitates the evaluation of many design changes without having to perform an experiment. The solver is capable of incorporating thermodynamic elements in a time-varying or steady state operating mode. A full description of NPSS and the NPSS system model will be presented in chapter 2 of the thesis.

While the NPSS model is a powerful design tool that can be used to explore a very wide parameter space, this type of modeling effort poses its own challenges and trade-offs. In particular, when combining many different levels of model fidelity among different model elements (combustion, cooling, separation, etc) additional considerations must be made and a "multi-disciplinary design optimization" or MDO should be considered [38]. NPSS allows the user to perform low level 'sensitivity analyses' that are a first step in this process. However the present work focuses on the development of the basic NPSS model and only presents results from a very narrow range of the parameter space that is centered around the ARL prototype design. A complete MDO of the propulsion system is a worthy objective but is beyond the scope of this thesis.

1.5 *Structure of the thesis*

Chapter 2 describes the general format of an NPSS element and how a system of multiple elements is solved. This is followed by a description of the models for each of the Aluminum combustion propulsion system's elements. Some are relatively simple, such as the fuel feeder. Others are more complex and rely on subroutine calls to separate programs under the NPSS framework. NPSS is described in detail in section 2.1. The reasons for using NPSS as opposed to developing our own code are presented. The embedded NPSS solver and how it solves our particular problem is discussed. Chapter 3 reports results from the NPSS performance simulations. These include basic predictions of power output and overall efficiency at the stated operating point as well as a preliminary sensitivity analysis. Chapter 4 presents the results of an analysis of predicted off-design performance. Chapter 5 presents conclusions about the operation of the system and proposals for future work with the NPSS model.

Chapter 2. Component Modeling

2.1 NPSS Structure and Solution Method
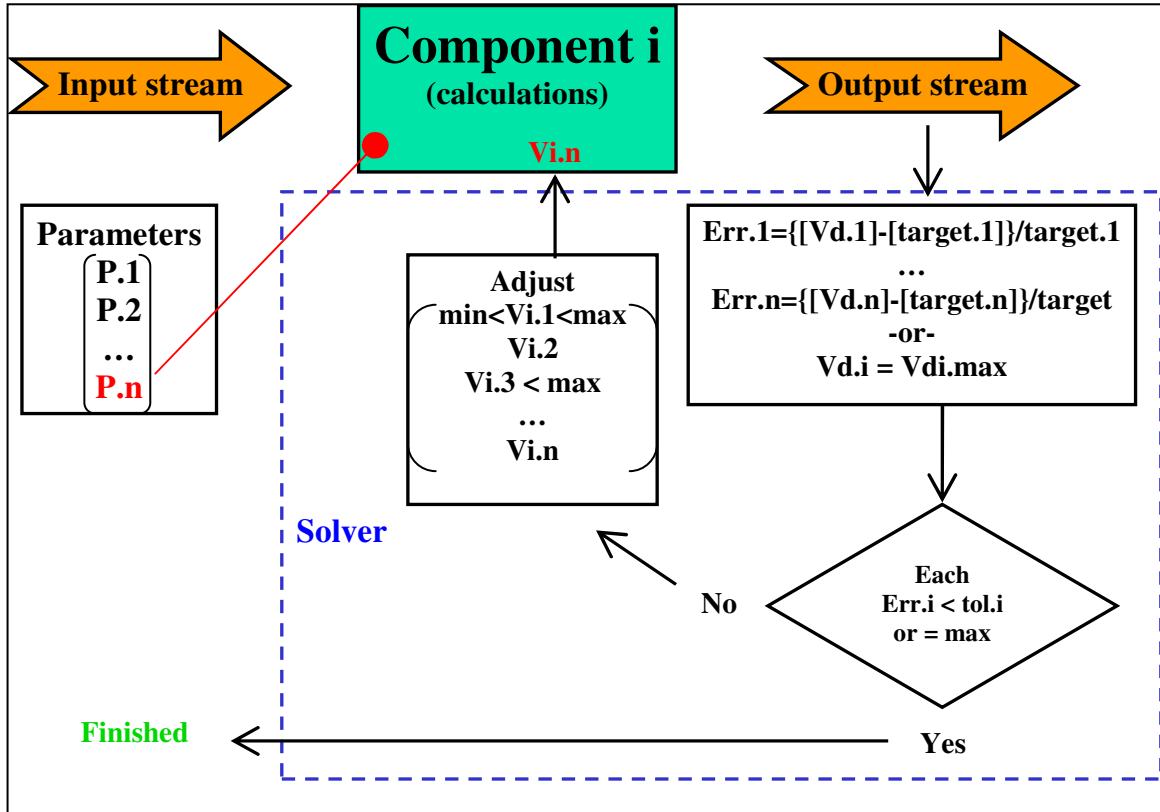
Figure 2.1 Component Structure

Input and Output 'streams' are NPSS data structures that contain and transfer physical attributes of the flow.   These include temperature, pressure, molecular weight, composition, etc. The model developed here uses three different types of streams: Fuel, Flow, and Shaft. Each has its own set of variables and function calls that describes the different attributes of its structure.   Figure 2.1 is a schematic illustration of how information is managed and flows in the NPSS environment.   A stream enters a component, has some or all of its attributes changed depending on the physical processes

occurring in the component, and exits the component with new values for some or all of its attributes. A stream originates from a 'flow start element' that establishes initial values of the stream's attributes.

'Parameters' (P.1, P.2…P.n) describe fixed attributes of a particular component that do not change during the solution process. Examples include the turbine efficiency or the flow area of a component. 'Independent Variables' (Vi.1, Vi.2…Vi.n) describe attributes of a particular component that are independently varied/controlled by NPSS in order to achieve a stable solution to the system. The independent variables in the Aluminum combustion system are the splitting ratios of the high temperature separator (β) and the quenching water (*BPR*), and the heat exchanger effectiveness (ε). It is also possible to impose maximum and/or minimum constraints that the independent variables can attain. An example would be limiting the temperature of the pre-combustor. All of the attributes in an output stream are 'dependent variables' (Vd.1, Vd.2…Vd.n) because they are the results of calculations that occurred within the element.

Figure 2.2 NPSS Model

17

Figure 2.2 shows the NPSS representation of the Aluminum combustion propulsion system where each element of the physical system is represented by a corresponding element in the NPSS framework. There are a few small differences between the simulated and actual system. First, the hydrogen recuperation system has been neglected in this analysis. This would require extra power to run, but it is expected to be a small fraction of the total power delivered. The simulation assumes an unlimited supply of both hydrogen and aluminum. In reality, the hydrogen is continually recycled through the cold loop separator and is required to fluidize the aluminum powder. Hydrogen generated during combustion would account for hydrogen lost in the separation processes and excess hydrogen could be stored on board for use in the startup. Second, the separator does not regenerate water to the pump. Third, all the water for combustion comes from outside at the ambient temperature. This assumption is valid assuming the condenser cold side is being operated at the ambient temperature. None of these simplifications should have a significant impact on the predicted power output and efficiency of the system.

Two additional flow start elements are required in order to account for the two flow loops that are present in the system. Flow start 1 is associated with the main loop of the power system. Flow start 2 is associated with the loop that re-circulates steam back to the combustor. These are non-physical elements in the sense that they do not have a direct analog in the physical system nor do they change any of the properties of the streams that pass through them. However, they are required in order to allow NPSS to find a solution. The system is solved by choosing a set of dependent variables whose target values are known. These target values are 'state points' of the system and are taken from reference values[39,40] and are included in the appendix. In this work, these are the recirculation

18

loop mass flow rate and temperature, and the temperature of the post-regenerator quenching water. They appear as blue text in figure 2.2. NPSS computes normalized errors for each of these variables based on the known state point values. In addition, NPSS computes the changes in mass flow and energy across the two flow start elements. Since these changes must be zero in order to satisfy conservation of mass, momentum, and energy, this leads to six more normalized error terms for a total of nine normalized error terms associated with the Aluminum combustion system.

NPSS solves the system by using a Newton-Rhapson method to adjust each Vi.x (in this case *BPR*, β, and ε) and the initial guesses for the temperature, pressure, and mass flow at each of the flow start elements in order to drive each of the nine components of the normalized error to zero. These dependent conditions are listed in table 2.1.

Independent	Dependent	Independent	Dependent
Pre-combustor Mass Flow (guess)	Pre-combustor Mass flow (calc)	Turbine Mass Flow (guess)	Turbine Mass Flow (calc)
Pre-combustor Temperature (guess)	Pre-combustor Temperature (calc)	Turbine Temperature (guess)	Turbine Temperature (calc)
Pre-combustor Pressure (guess)	Pre-combustor Pressure (calc)	Turbine Pressure (guess)	Turbine Pressure (calc)
Splitter Bypass Ratio (BPR)	Recirculation Mass Flow	Separator Bypass (β)	Recirculation Temperature
Heat Exchanger Effectivenesss (ε)	Quenching Water Temperature		

2.1 Independent and Dependent Variables

19

The independent variables appear as red text in figure 2.2. Constraints can be applied to represent physical limitations of the system such as maximum burner output temperature. Additional description of the solution process is presented in Chapter 3.

Sections 2.2-2.12 of this report present the various parameters, variables, constraints, and error terms which are used to describe each component in NPSS. The thermodynamic calculations performed by each element are presented along with the attendant simplifications, governing equations, and assumptions. The actual NPSS code for each element is presented in Appendix 1.

Symbol	Quantity
Name.Fl_I	NPSS Fluid element input
Name.Fl_O	NPSS Fluid element output
Name.Fl_I.x	x can be:
P	Pressure
T	Temperature
W	Weight flow
Mf	Mass fraction
Y	Mole fraction
Ht	Specific enthalpy
S	Specific entropy
Name.Sh_I	NPSS Shaft element input
Name.Sh_O	NPSS Shaft element output
Name.Sh_O.pwr	Shaft power

Table 2.2   NPSS Nomenclature

A brief overview of the nomenclature listed in Table 2.1 will facilitate understanding of the NPSS code provided in the appendix as well as in the element model descriptions where NPSS shorthand is sometimes substituted. "Name" in this case refers to a model element. The syntax 'Name.x' is common when used in reference to C++ structures: In this case each element is a C++ structure where Name.Fl_I is the fluid input and Name.Fl_O is the fluid output. Properties of the fluid can be further accessed by using 'Name.Fl_I.x' where x is any of the listed values. NPSS uses a different structure to describe mechanical linkages between turbines and compressors with their drive shafts. In this work the shaft power, Name.Sh_O.pwr is the only relevant output. See the NPSS Users Guide [41] or Developers Guide [41] for more information on NPSS nomenclature.

2.2 *Flow Start*
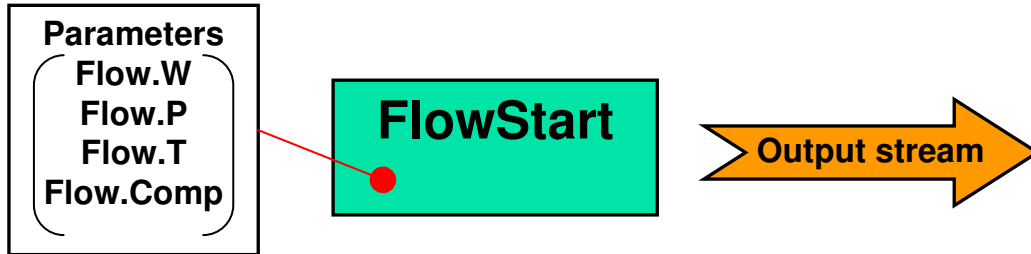
Figure 2.3 Flow Start Element Diagram

Flow Start:

Parameters	Symbol	Units
Weight Flow	$Flow.W$	lb/s
Pressure	$Flow.P$	psia
Temperature	$Flow.T$	Fahrenheit
Composition	$Flow.setComp(X)$	X is a molecule type

Variables	Symbol	Units
None		

Constraints	Symbol	Units
None		

Governing Equations:

22

Parameters	Symbol	Units
None		

Error Terms:

Parameters	Symbol	Units
None		

Method of Solution:

This element feeds a flow of some molecular composition at a specified mass flow, temperature and pressure. In the physical system, this accounts for the hydrogen fed to the fuel seeder system as well as the ambient water source flow.

2.3   *Aluminum Fuel Seeder Element Model*

Schematic Diagram:
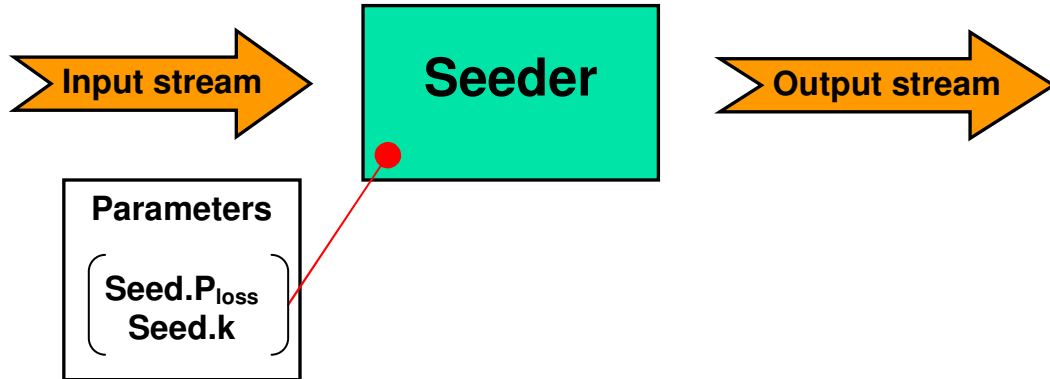
Figure 2.4 Seeder Element Diagram

Assumptions:

- Exit pressure is sufficiently large to choke the flow from seeder to combustor so that disturbances in the combustor are unable to affect the seeder.

- Input gas is assumed to be hydrogen gas entering at known temperature, pressure, and weight flow rate.

- The details of the particle entrainment process occurring in the seeder are ignored. Instead, a simple ratio of the flow of aluminum to the flow of hydrogen is used to model flow seeding.

- Seeder performance depends only on the Entrainment Ratio, k_{seed}, and the Pressure Loss, dP_{seed}. (NOTE: At the top in your intro, you used a colon after statements prior to their corresponding formulas. Do you want to do that or a period? Pick one or the other. I corrected it so that each section throughout is consistent within itself, but it should be consistent for the whole paper.)

$$k_{seed} = \frac{w_{al}}{w_{H_2}} \qquad dP_{seed} = \frac{P_2}{P_1}$$

- There are no other viscous losses in the seeder, no heat loss due to conduction through the walls (adiabatic), and the pressure lost by the hydrogen to entrain the aluminum does not cause the temperature of the gas to drop significantly.

$$\dot{Q}_{loss} = 0 \qquad T_2 = T_1$$

- The fluid experiences negligible changes in kinetic and potential energy as it passes through the seeder.

$$V_1^2 - V_2^2 = 0 \qquad g(z_1 - z_2) = 0$$

- The seeder is operating in steady state; no transient effects are considered.

- Complex mixture effects have been neglected [43]. Therefore, the mixture is assumed to be homogeneous with hydrogen and aluminum transported at the mixture velocity and temperature.

$$V_i = V_{mix} \qquad T_i = T_{mix}$$

- The subscripts 1 and 2 refer to properties measured at the component inlet and outlet respectively.

Seeder:

Parameter	Symbol	Units
Entrainment Ratio	k_{seed}	None
Pressure Ratio	dP_{seed}	None

Variable	Symbol	Units
None		

Constraint	Symbol	Units
None		

Governing Equations:

Conservation of mass	$\dot{w}_{in} = \dot{w}_{out}$	(2.3.1)

Error Terms:

Parameter	Symbol	Units
None		

Method of Solution:

The function of the flow seeder is to use high pressure hydrogen gas to fluidize the solid

aluminum particles and transport them to the combustor. Fluidization occurs via the

26

transfer of momentum to the aluminum from the hydrogen. However, the 3-D Navier-Stokes equations that would need to be solved to find the mixture exit velocity are too complex for this analysis. Instead, the output weight flow is determined using mass conservation. The entrainment ratio k_{seed}, which describes the seeding performance, is assumed to be known.

$$\dot{w}_2 = \dot{w}_1 (1 + k_{seed})$$ (2.3.2)

Similarly, the exit pressure is determined using the pressure ratio dP_{seed} which is assumed to be known.

$$P_2 = P_1 * dP_{seed}$$ (2.3.3)

2.4   *Re-circulated Flow Start*

Schematic Diagram:
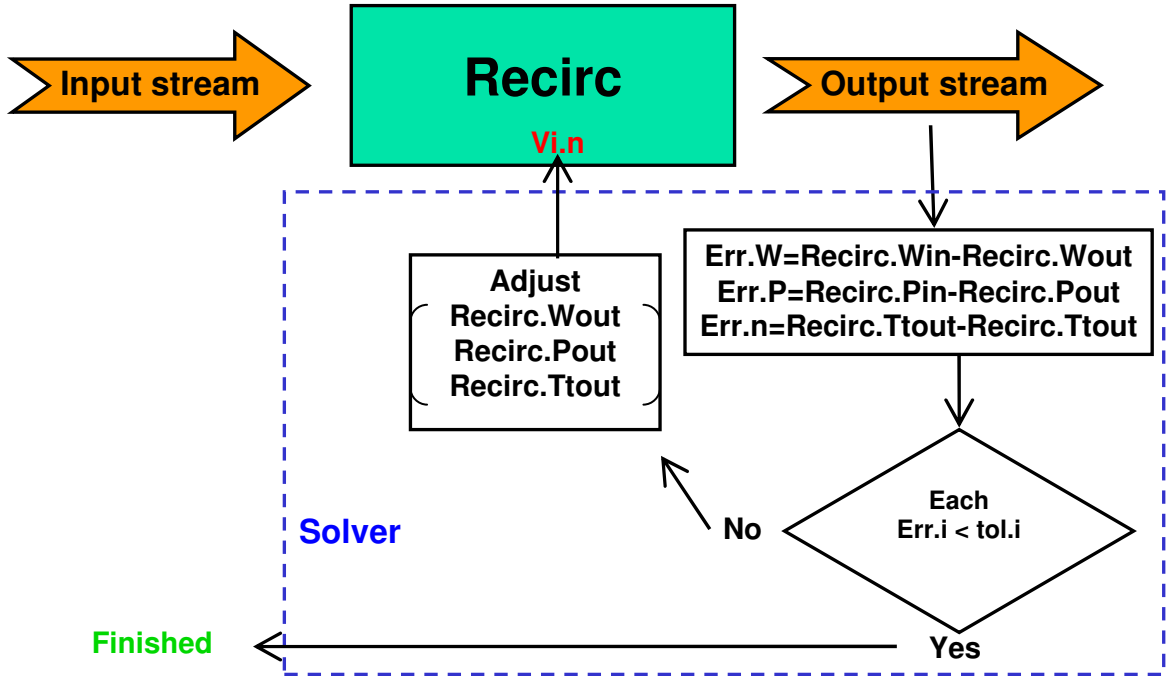
Figure 2.5 Recirculation Element Diagram

Assumptions:

- This element generates a guess of the output values to permit the solution to proceed.

- The composition of the constituent gasses (ratio of molecules) is a known fixed parameter.

- The recirculation is considered pure gaseous water in this case.

Re-circulated Flow Start:

Parameter	Symbol	Units
Composition	$Flow.setComp(X)$	X is a molecule type

Variables	Symbol	Units
Mass Flow Out	$\mathrm{Re}\,circ.Fl\_O.W$	lb/s
Pressure Out	$\mathrm{Re}\,circ.Fl\_O.Pt$	Psia
Temperature Out	$\mathrm{Re}\,circ.Fl\_O.Tt$	Fahrenheit

Constraint	Symbol	Units
None		

Governing Equations:

Conservation of mass	$\dot{w}_{in} = \dot{w}_{out}$	(2.4.1)

Error Terms:

Term	Equation	Units
Mass Flow Error	$\mathrm{Re}\,circ.Fl\_O.W - \mathrm{Re}\,circ.Fl\_I.W$	lb/s
Pressure Error	$\mathrm{Re}\,circ.Fl\_O.Pt - \mathrm{Re}\,circ.Fl\_I.Pt$	Psia
Temperature Error	$\mathrm{Re}\,circ.Fl\_O.Tt - \mathrm{Re}\,circ.Fl\_I.Tt$	Fahrenheit

Method of Solution:

The recirculation element is required to perform closed loop analyses in NPSS. Its purpose is to allow elements which rely on downstream data to use a guess of the values of mass flow, pressure and temperature at the upstream location. After the downstream flow variables are computed, the resulting values are compared to the initial guesses. If the normalized errors are not less than the tolerances, the system uses an intermediate guess and re-computes the solution. This convergence process is controlled by the Newton-Raphson solver built into NPSS.

2.5 *Combustor Element Model*

Schematic Diagram:
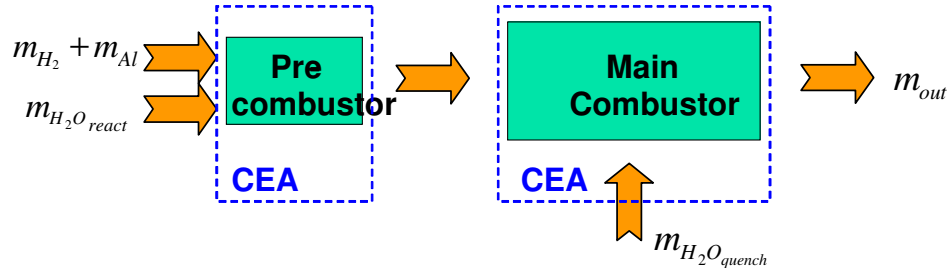
Figure 2.6 Combustor Element Diagram

Assumptions:

- Inlet mass flows, temperature and pressures are known for the aluminum-hydrogen stream as well as the pressurized water stream.

- Combustor pressure is specified.

$$P_{combust}$$

- A CEA equilibrium calculation is used to determine the composition of the products and the heat of combustion. Reaction rates are not computed. The balanced chemical reaction for aluminum reacting with water is shown below.

$$2Al + 3H_2O + (8H_2O + 2.7H_2) \Rightarrow Al_2O_3 + 3H_2 + (8H_2O + 2.7H_2)$$
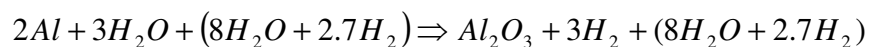
Note: This reaction carried additional water to "quench" the combustion reaction that was listed in the Introduction. Adding more water lowers the temperature of the combustor and creates steam via direct contact of liquid water and the hot products in the combustor. It is this additional steam which provides power generation in the system via the turbine.

- Heat losses to the environment are a known parameter.

$$\dot{Q}_{loss}$$

- The fluid experiences negligible changes in kinetic and potential energy as it passes through the combustor.

$$V_1^2 - V_2^2 = 0 \qquad g(z_1 - z_2) = 0$$

- Complex mixture effects like the partial pressure of aluminum and alumina have been neglected [43]. The mixture is assumed to be homogeneous so that water, hydrogen and aluminum/alumina are transported at the mixture velocity and temperature.

$$V_i = V_{mix} \qquad T_i = T_{mix}$$

- The subscripts 1, 2, 3 and 4 refer to properties measured at the inlet for hydrogen-aluminum, steam, liquid water and the combustor exit respectively.

Combustor:

Parameter	Symbol	Units
Combustion Pressure	$P_{combust}$	Psia

Variables	Symbol	Units
None		

Constraint	Symbol	Units
None		

Governing Equations:

Conservation of mass	$\dot{w}_{in} = \dot{w}_{out}$	(2.5.1)
Energy	$\dot{E}_{in} = \dot{E}_{out}$ $\dot{E} = \dot{Q} + \dot{W} + \sum m_i \dot{w}\left(h_i + \dfrac{V_i^{\,2}}{2} + gz_i \right)$	(2.5.2)
Steady Flow Reaction	$\sum_i \dot{n}_r \left(\overline{h}_f^0 + h - h^0 \right)_r = \sum_i \dot{n}_p \left(\overline{h}_f^0 + h - h^0 \right)_p$	(2.5.3)
Gibbs Free Energy	$g = \sum\limits_{i=1}^{numspecies} n_i \left(\dfrac{dg}{dn} \right)_{T,P,n}$	(2.5.4)

Error Terms:

Term	Equation	Units
None		

Method of Solution:

The chemical reaction proscribed for the combustion of aluminum with additional sea water is given by:

$$2Al + 3H_2O + \left(8H_2O + 2.7H_2 \right) \Leftrightarrow Al_2O_3 + 3H_2 + \left(8H_2O + 2.7H_2 \right) \quad (2.5.5)$$
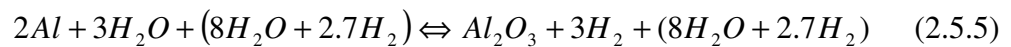
CEA computes the heat release and the equilibrium composition of the products by minimizing the Gibbs free energy of the mixture. For a detailed description see Gordon

and McBride [8]. CEA determines the final temperature of the mixture by solving for the

equilibrium heat release for a steady flow reaction (2.4.3). In this expression, $\left(\bar{h}_f^0\right)_r$ is the

standard enthalpy of formation for reactant r at reference temperature, T_{ref}, usually 298K.

To compensate for the true enthalpy, h, of the incoming reactant, a correction, $h - h^0$ is

applied where h^0 is the enthalpy at the reference temperature, T_{ref}. The change in

enthalpy of the mixture is the net heat of reaction and CEA uses an iterative procedure to

determine the final temperature of the mixture.

A sample CEA calculation appears below where the initial conditions are the input

weight flows and temperatures taken from [40]. Results corresponding to two different

combustor exit pressures, ☐ psi from [40] and ☐ psi are presented.

	Weight flow (lb/s)	Temperature (F)
H_2		
AL		
H_2O		
H_2O(l)		

Table 2.3 Reactants for CEA sample calculation

Al	AlH	AlO	AlOH	AlO_2	AlO_2H
Al_2	Al_2O	Al_2O_2	*H	HAlO	HO_2
H_2	H_2O_2	*O	*OH	$*O_2$	O_3
Al(l)	Al_2O_3(s)	Al_2O_3(l)	H_2O(g)	H_2O(s)	H_2O(l)

Table 2.4 Species being considered in this system
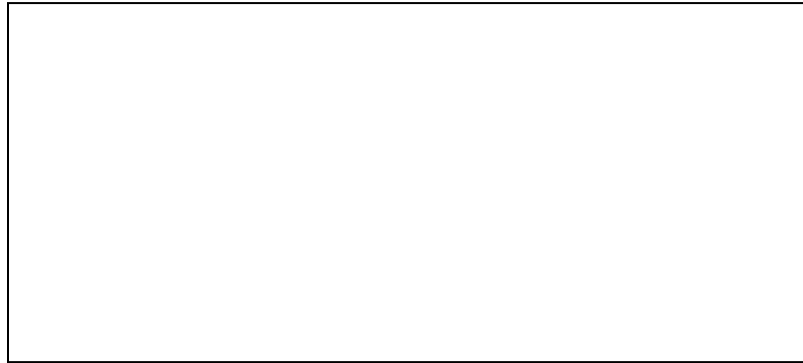
Table 2.5 Sample CEA Input File

The CEA output is presented below. The first section of the output file shows the initial conditions for the calculation. The second section of the output file shows the output conditions at ___ psi (first column) and ___ psi (second column).

```
THERMODYNAMIC EQUILIBRIUM COMBUSTION PROPERTIES
AT ASSIGNED PRESSURES
CASE = Point-1
               REACTANT            WT FRACTION   ENERGY    TEMP
                                                 CAL/MOL     K
FUEL      H2
FUEL      AL(cr)
FUEL      H2O
FUEL      H2O(L)


P, ATM
T, K
RHO, G/CC
H, CAL/G
U, CAL/G
G, CAL/G
S, CAL/(G)(K)

M, (1/n)
MW, MOL WT
(dLV/dLP)t
(dLV/dLT)p
Cp, CAL/(G)(K)
GAMMAs
SON VEL,M/SEC

MOLE FRACTIONS
*H2
H2O
AL2O3(a)
```

Table 2.6 Sample CEA Output File

The results show that the equilibrium temperature is [_____], which is lower than

the combustion temperature of [_____] reported in Ref. 40. This discrepancy is likely due

to the nominal rate of H_2O addition which is not explicit in Ref. 40. Note the mixed units

in the output (English and SI). CEA will do calculations in any units you give it as long

as you tell it what they are and you choose a consistent system. Quantities are returned in

the same units given. If no units are specified, CEA defaults to English units.

2.6 *Separator Element Model*

Schematic Diagram:
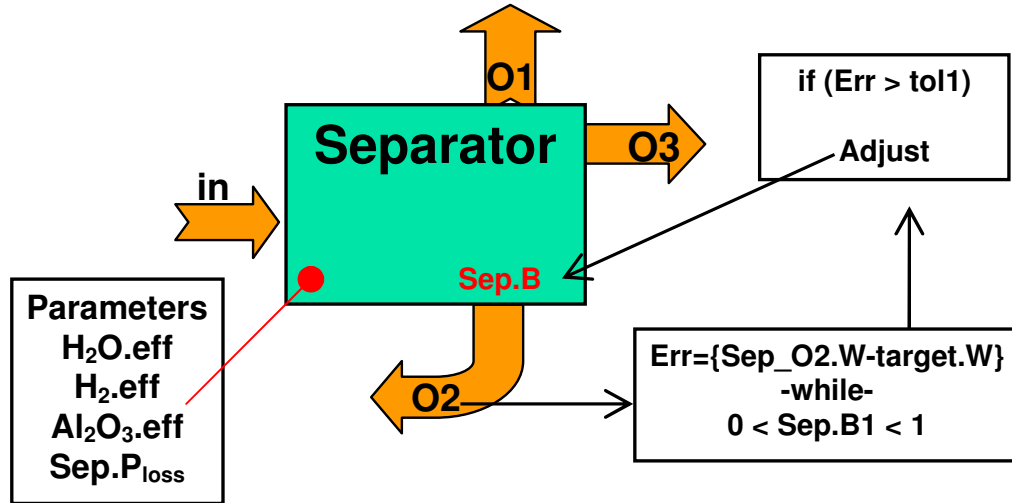
Figure 2.7 Separator Element Diagram

Assumptions:

- The total temperature T_0 and the mole fractions y_i of the inputs are known.

- The subscripts '*in*', *1*, *2*, and *3* refer to properties measured at the component inlet, overboard solid particle, recirculated steam, and turbine power stream respectively.

- The subscript *i* refers to the individual species being considered. In this case, *i=1* corresponds to H_2O, *i=2* corresponds to H_2 and *i=3* corresponds to Al_2O_3,

- The amount of work required to separate a mixture into its pure components is equal to the ideal reversible work produced by mixing.

$$W_{rev} = -R_u T \sum_i^n N_i \ln y_i$$

37

- There is no work input to the separator, thus all work performed to separate the mixture comes from the input stream.

- The separation efficiency for each of the constituents is given by:

$$\eta_{Al} = \frac{\dot{w}_{Al,3}}{\dot{w}_{Al,1}} \qquad \eta_{H2O} = \frac{\dot{w}_{H2O,3}}{\dot{w}_{H2O,1}} \qquad \eta_{H2} = \frac{\dot{w}_{H2,3}}{\dot{w}_{H2,1}}$$

- Although the separation of aluminum oxide is never 100%, the remaining fraction has a negligible affect on the thermodynamic process since the solid does not contribute to the pressure, nor does it have thermal mass enough to significantly affect the temperature of the mixture.

- The separation process occurs adiabatically.

Separator:

Parameter	Symbol	Units
H_2O Separator efficiency	η_{H2O}	None
Al_2O_3 Separator efficiency	η_{Al2O3}	None
H_2 Separator efficiency	η_{H2}	None

Variables	Symbol	Units
Recirculation Bypass	β	None

Constraints	Symbol	Value
Bypass max	β max	1
Bypass min	β min	0

Governing Equations:

Ideal Gas Equation of State	$Pv = RT$	(2.6.1)
Conservation of mass	$\dot{w}_{in} = \dot{w}_{out}$	(2.6.2)
Conservation of Energy	$\dot{E}_{in} = \dot{E}_{out}$ $$E = \dot{Q} + \dot{W} + \sum m_i \dot{w}\left(h_i + \frac{V_i^2}{2} + gz_i \right)$$	(2.6.3)
Entropy	$$\Delta s = \int_{T_1}^{T_2} C_p \frac{dT}{T} - \int_{P_1}^{P_2}\left(\frac{\partial v}{\partial T} \right)_P dP$$	(2.6.4)

Error Terms:

Term	Equation	Units
Recirculated Mass Flow	$\mathrm{Re}\,circ_{Actual}.Fl\_O.W - \mathrm{Re}\,circ_{T\arg et}.W$	lb/s

Method of Solution:

The process of mixing generates entropy [44]. For a process involving n components, the entropy generated is given by: [44]

$$S_{gen} = -R_u \sum_i^n N_i \ln y_i \qquad (2.6.6)$$

The amount of work that is lost during a mixing process can be determined by the product of the entropy generated and the temperature of the surroundings in which mixing took place.

$$W_{lost} = T_{env} S_{gen} \qquad (2.6.6)$$

Separation is a mixing process occurring in reverse. Therefore, the amount of work required to completely separate the components of a mixture into its components is, at least:

$$W_{separation} = -R_u T \sum_i^n \dot{N}_i \ln y_i \tag{2.6.7}$$

Since the hydrogen and steam remain mixed, the minimum work required to separate the aluminum oxide from the steam and hydrogen is the difference between the work associated with complete separation of the incoming gas mixture and that associated with the separation of the output stream mixture. Therefore:

$$\dot{W}_{separation} = -R_u T \sum_{i=1}^3 \dot{N}_{i,1} \ln y_{i,1} + R_u T \sum_{i=1}^3 \dot{N}_{i,2} \ln y_{i,2} \tag{2.6.8}$$

where $i=1$ corresponds to Al_2O_3, $i=2$ corresponds to H_2O, and $i=3$ corresponds to H_2. Re-writing 2.6.8 in terms of the weight flow and the molecular weight of species i, MW_i gives:

$$\dot{W}_{separation} = -R_u T \sum_{i=1}^3 \frac{\dot{w}_{i,1}}{g} MW_i \ln y_{i,1} + R_u T \sum_{i=1}^3 \frac{\dot{w}_{i,2}}{g} MW_i \ln y_{i,2} \tag{2.6.9}$$

Conservation of mass is used to determine the weight flow rates of the individual species exiting the control volume through the two discharges, gas-phase and solid-phase:

$$\dot{w}_{i,2} = \dot{w}_{i,1}(1 - \eta_i) \tag{2.6.10}$$

$$\dot{w}_{i,3} = \dot{w}_{i,1}\eta_i \tag{2.6.11}$$

The mole fractions in the outlet streams are determined from the flow rates of the individual species:

$$y_{i,2} = \frac{\dfrac{w_{i,2}}{g} MW_i}{\displaystyle\sum_{i=1}^{3} \frac{w_{i,2}}{g} MW_i} \qquad y_{i,3} = \frac{\dfrac{w_{i,3}}{g} MW_i}{\displaystyle\sum_{i=1}^{3} \frac{w_{i,3}}{g} MW_i} \qquad (2.6.12, \ 2.6.13)$$

The output enthalpy is determined using conservation of energy for an adiabatic process:

$$\sum_{i=1}^{3} mf_{i,1} \dot{w}_1 h_{i,1} = \dot{W}_{separation} + \sum_{i=1}^{3} mf_{i,2} \dot{w}_2 h_{i,2} + \sum_{i=1}^{3} mf_{i,3} \dot{w}_3 h_{i,3} \qquad (2.6.14)$$

The total system enthalpy is a mass weighted average of the individual component enthalpies evaluated at the temperature and pressure of the mixture. Therefore, the temperatures of the components exiting the separator decrease in order to compensate for the separation enthalpy. The enthalpies of each component are found using the reference tables generated by CEA. It is assumed that the separation of aluminum oxide from the hydrogen steam flow occurs very quickly so that the enthalpy of the components exiting through port 3 remain unchanged from their values as they enter through port 1. Assuming that the portion of aluminum oxide that escapes through port 2 is thermodynamically insignificant allows us to drop those terms from equation 2.6.14, which becomes:

$$\sum_{i=1}^{2} mf_{i,1} \dot{w}_2 h_{i,1} = \dot{W}_{separation} + \sum_{i=1}^{2} mf_{i,2} \dot{w}_2 h_{i,2} \qquad (2.6.15)$$

Rearranging 2.6.15 to solve for the loss in enthalpy, and assuming that the total mixture leaving via stream 2 is at the same temperature, introduces a new parameter, α, which will enable an iterative solution:

$$\alpha = \frac{\Delta h_{H_2O}}{\dot{W}_{separation}} \qquad (2.6.16)$$

41

$\alpha = 1$ implies that all of the work of separation is from a loss in enthalpy of the water, and a $\alpha = 0$ implies that all the work of separation is from a loss in enthalpy of the hydrogen. The output states can then be individually computed based on a guess of phi:

$$mf_{H_2,2} \dot{w}_2 h_{H_2,1} - (1-\alpha)\dot{W}_{separation} = mf_{H_2,2} \dot{w}_2 h_{H_2,2} \tag{2.6.17}$$

$$mf_{H_2O,2} \dot{w}_2 h_{H_2O,1} - \alpha\dot{W}_{separation} = mf_{H_2O,2} \dot{w}_2 h_{H_2O,2} \tag{2.6.18}$$

Assuming ideal gas behaviors for high temperatures and relatively low pressures:

$$T_{H_2,2} = \frac{mf_{H_2,2} \dot{w}_2 Cp_{H_2} T_1 - (1-\alpha)\dot{W}_{separation}}{mf_{H_2,2} \dot{w}_2 Cp_{H_2}} \tag{2.6.19}$$

$$T_{H_2O,2} = \frac{mf_{H_2O,2} \dot{w}_2 Cp_{H_2O} T_1 - \alpha\dot{W}_{separation}}{mf_{H_2O,2} \dot{w}_2 Cp_{H_2O}} \tag{2.6.20}$$

The true solution will be the α value for which the temperatures of both components are equal.

2.7   *Turbine Element Model*

Schematic Diagram:
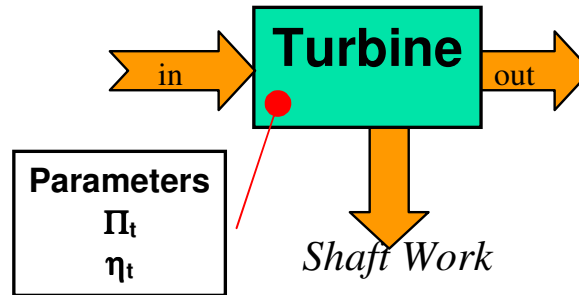
Figure 2.8 Turbine Element Diagram

Assumptions:

- All inputs and outputs are assumed to be ideal mixtures of real gases. This means that all gasses in the system are treated as 'non-ideal' for the purpose of calculating their properties but that the mixture is 'ideal' in the sense that mixing does not change the enthalpies of the individual components. Therefore:

$$\Delta H_{mixing} = 0 \qquad h_{mixture} = \sum h_i(T_m, P_m) \qquad s_{mixture} = \sum s_i(T_m, P_i)$$

- Turbine performance depends only on the pressure ratio Π_t and the isentropic efficiency η_t.

$$\Pi_t = \frac{P_2}{P_1} \qquad \eta_T = \frac{h_1 - h_2}{h_1 - h_{2s}} = \frac{W_{actual}}{W_{ideal}}$$

- There are no losses due to friction in the turbine and no heat loss due to conduction through the walls (adiabatic).

$$\dot{Q}_{loss} = 0$$

43

- The fluid experiences negligible changes in kinetic and potential energy as it passes through the turbine.

$$V_1^2 - V_2^2 = 0 \qquad g(z_1 - z_2) = 0$$

- The mixture is assumed to be homogeneous with all components traveling at the mixture velocity.

$$V_i = V_{mix} \qquad T_i = T_{mix}$$

- The concentration of particulate aluminum is small, has zero partial pressure, and therefore does not contribute to the total entropy.

$$P_{Al_2O_3} = 0 \qquad s_{Al_2O_3} = 0$$

- The subscripts 1 and 2 refer to properties measured at the component inlet and exit respectively.

- No phase changes occur in the turbine.

Turbine:

Parameter	Symbol	Units
Turbine Pressure Ratio	Π_t	None
Isentropic Efficiency	η_t	None
Shaft RPM	$\dot{\theta}$	Rev/min

Variables	Symbol	Units
None		

Constraints	Symbol	Value

None		

Governing Equations:

Conservation of mass	$\dot{w}_1 = \dot{w}_2$	(2.7.1)
Conservation of Energy	$\dot{E}_1 = \dot{E}_2$ $\dot{E} = \dot{Q} + \dot{W} + \sum_{i=1}^{n} m_i \dot{w}\left(h_i + \frac{V_i^2}{2} + gz_i \right)$	(2.7.2)
Dalton's law	$P = \sum_{i=1}^{n} P_i\left(T_{mix}, V_{mix}\right)$	(2.7.3)
Ideal Gas Equation of State	$Pv = RT$	(2.7.4)
Ideal Gas Specific Heats	$dh = C_p(T)dT$	(2.7.5)
Gibbs Equation	$Tds = du + Pdv$	(2.7.6)
Real Gas Enthalpy	$\Delta h = \int_{T_1}^{T_2} C_p \, dT + \int_{P_1}^{P_2}\left[v - T\left(\frac{\partial v}{\partial T}\right)_P \right] dP$	(2.7.7)
Real Gas Entropy	$\Delta s = \int_{T_1}^{T_2} C_p \frac{dT}{T} - \int_{P_1}^{P_2}\left(\frac{\partial v}{\partial T}\right)_P dP$	(2.7.8)

Error Terms:

Term	Equation	Units
None		

Method of Solution:

Shaft work output:

From conservation of energy (2.7.2) and the assumptions listed above, the shaft work produced by the turbine is:

$$\dot{W} = \dot{w}(h_1 - h_2) \tag{2.7.9}$$

h is the enthalpy per unit mass, which is determined using the mixture temperature, pressure, and composition and equations 2.7.3 – 2.7.7. However, computing the enthalpy per unit mass in this way for each run is computationally inefficient. Instead, lookup tables of enthalpy as a function of temperature, pressure, and mixture weight fraction are generated ahead of time for use in the calculations. An example is presented in table 2.7.

Reactant	Weight Fraction	Energy kJ/mol	Temperature K
H$_2$			
AL			
H$_2$O			
H$_2$O(l)			
P (atm)			
T (K)			
RHO (kg/m^3)			
H (kJ/kg)			
U (kJ/kg)			
G (kJ/kg)			
S (kJ/kgK)			

Table 2.7 Thermodynamic Properties of a mixture of H$_2$, Al, and H$_2$O; (6)

Table 2.7 is generated by NPSS by calling CEA, one of its standard thermodynamics packages. The following NPSS command is used to set the total state of the mixture entering the turbine by interpolating in the database:

$$Fl.I.setTotal\_TP(T_1, P_1) \qquad (2.7.10)$$

The enthalpy and entropy entering the turbine are retrieved using the following NPSS commands:

$$h_1 = Fl.I.ht \qquad (2.7.11)$$

$$s_1 = Fl.I.S \qquad (2.7.12)$$

The turbine exit pressure is computed using the inlet pressure and the turbine pressure ratio:

$$P_2 = \Pi_t \times P_1 \qquad (2.7.13)$$

Conservation of mass (2.7.1) and the assumption that no phase changes occur within the turbine indicate that the composition of the liquid-vapor mixture entering the turbine is the same as that leaving the turbine. This enables us to temporarily "copy" all of the parameters describing the entrance flow to the exit:

$$Fl.O.copyFlow("Fl.I") \qquad (2.7.14)$$

A second NPSS call to CEA computes the state of the mixture that would result if the expansion through the turbine were isentropic (ie. $s_2=s_1$):

$$Fl.O.setTotalSP(s_1, P_2) \qquad (2.7.15)$$

This enables us to determine h_{2s} as follows:

$$h_{2s} = Fl.O.ht \qquad (2.7.16)$$

The actual enthalpy of the mixture exiting the turbine is determined using the definition of the turbine efficiency:

47

$$h_2 = h_1 - \eta_T (h_1 - h_{2s})$$ (2.7.17)

The conditions of the mixture exiting the turbine are updated using another NPSS call to CEA based on the pressure computed in 2.7.13 and the enthalpy computed in 2.7.17.

$$Fl.O.setTotal\_htP(h_2, P_2)$$ (2.7.18)

Finally, NPSS computes the shaft power ($\dot{W}_s$) using equation 2.7.9.

2.8 Regenerator Element Model

Schematic Diagram:
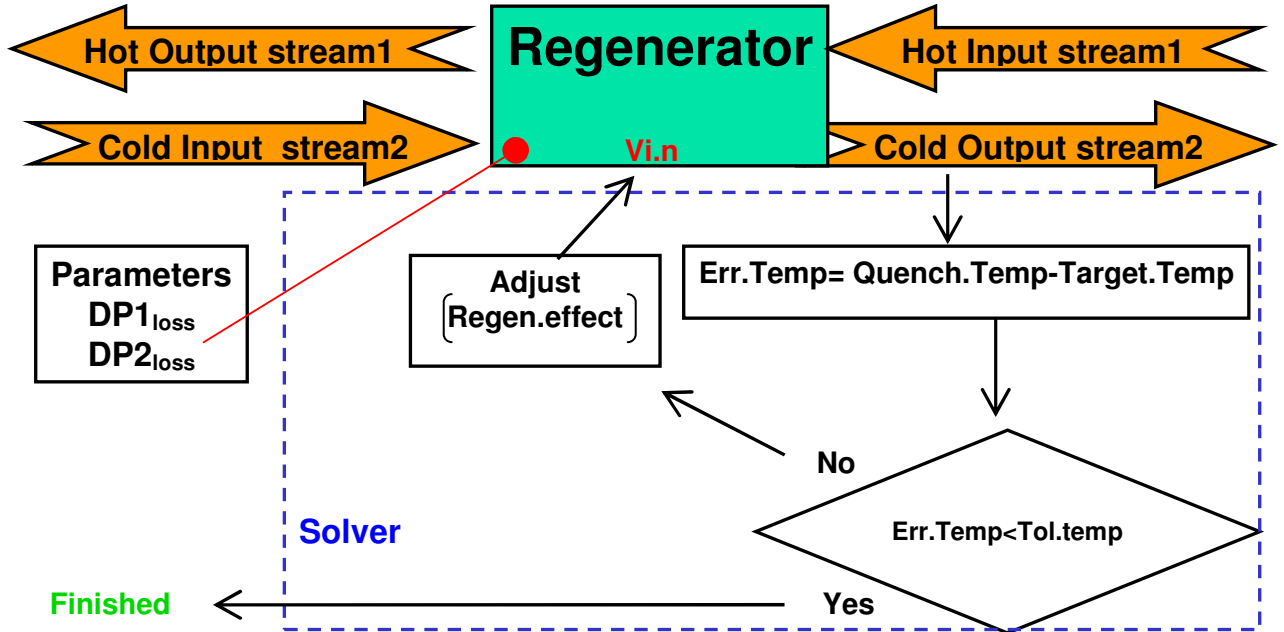
Figure 2.9 Regenerator Element Diagram

Assumptions:

- Regenerator performance depends only on the regenerator effectiveness, ε_R and

  pressure drop on each side dP_1 and dP_2.

$$\varepsilon_R = \frac{q_{regen,act}}{q_{regen,\max}} = \frac{h_{precombust} - h_{pump}}{h_{turbine,out} - h_{pump}} = \frac{h_4 - h_3}{h_1 - h_3}$$

$$dP_1 = \frac{P_{1,out}}{P_{1,in}}$$

$$dP_2 = \frac{P_{2,out}}{P_{2,in}}$$

49

- There are no viscous losses in the regenerator and no heat loss due to conduction through the walls, i.e. the overall system is adiabatic in the sense that all heat lost from one stream is gained by the other.

$$\dot{Q}_{loss} = 0$$

- The fluid experiences negligible changes in kinetic and potential energy as it passes through the regenerator.

$$V_1^{\,2} - V_2^{\,2} = 0$$
$$g(z_1 - z_2) = 0$$

- The subscripts 1, 2, 3 and 4 refer to properties measured at the hot inlet and exit and cold inlet and exit respectively.

- The flow through the cold side is assumed to be single phase (liquid).

Regenerator Element:

Parameter	Symbol	Units
Hot side pressure ratio	dP_1	None
Cold side pressure drop	dP_2	None

Variable	Symbol	Units
Regenerator effectiveness	ε_R	None

Constraints	Symbol	Value
None		

Governing Equations:

Conservation of mass	$\dot{w}_{in} = \dot{w}_{out}$	(2.8.1)
Energy	$\dot{E}_{in} = \dot{E}_{out}$ $E = \dot{Q} + \dot{W} + \sum m_i \dot{w}\left(h_i + \dfrac{V_i^2}{2} + gz_i\right)$	(2.8.2)
Enthalpy	$\Delta h = \int\limits_{T_1}^{T_2} C_p \, dT + \int\limits_{P_1}^{P_2}\left[v - T\left(\dfrac{\partial v}{\partial T}\right)_P\right]dP$	(2.8.3)

Error Terms:

Term	Equation	Units
Quenching Water Temperature	$\mathrm{Re}\, gen_{Actual}.Fl\_02.Tt - \mathrm{Re}\, gen_{T\arg et}.T$	Fahrenheit

Method of Solution:

In this power system, the residual enthalpy of the steam/hydrogen mixture exiting the turbine is recovered by using it to pre-heat the water entering the combustor. This decreases the amount of fuel required to achieve combustion temperatures thereby improving the overall thermal efficiency of the system.

The temperature of the hot gasses entering from the turbine sets the maximum possible temperature to which the water entering the cold side of the regenerator can be raised. The degree to which the cold side water stream is pre-heated is calculated using the definition of regenerator effectiveness and the turbine exit and pump exit enthalpies, h_1 and h_3 respectively:

$$h_4 = h_3 + \varepsilon_R\left(h_1 - h_3\right) \tag{2.8.4}$$

Note that h_3 is determined using T_3, the pump exit temperature, and the enthalpy look-up tables for sea water. Conservation of energy for the entire regenerator is used to determine h_2:

$$h_2 = h_1 - \left(h_4 - h_3\right) \tag{2.8.5}$$

The exit pressures for each stream are calculated using the prescribed pressure drops:

$$p_2 = p_1 \cdot dP_1 dq \tag{2.8.6}$$

$$p_4 = p_3 \cdot dP_3 dq \tag{2.8.7}$$

NPSS is used to set the final output state of the flow based on the exit enthalpies and pressures of each stream: $H.Fl.O.setTotal\_htP(h_2, p_2)$ \hfill (2.8.8)

$$C.Fl.O.setTotal\_htP(h_4, p_4) \tag{2.8.9}$$

Note that in order not to violate the assumptions of single-phase flow in the hot side, the regenerator should be sized so that condensation does not occur on the hot side. This restriction imposes an effective limit on the maximum possible heat transfer. This limit is determined using the following procedure.

The maximum heat transfer occurs when enough heat is removed to bring the turbine stream to the saturation temperature:

$$h_4 - h_3 = \left(h_1 - h_2\right) \le h_1 - h_{2,sat} \tag{2.8.10}$$

Therefore, the constraint on the regenerator's effectiveness required to not violate the assumption of single phase flow in the hot side is given by:

$$\varepsilon_R \le \frac{h_1 - h_{2,sat}}{h_1 - h_3} \tag{2.8.11}$$

2.9 *Condenser Element Model*

Schematic Diagram:
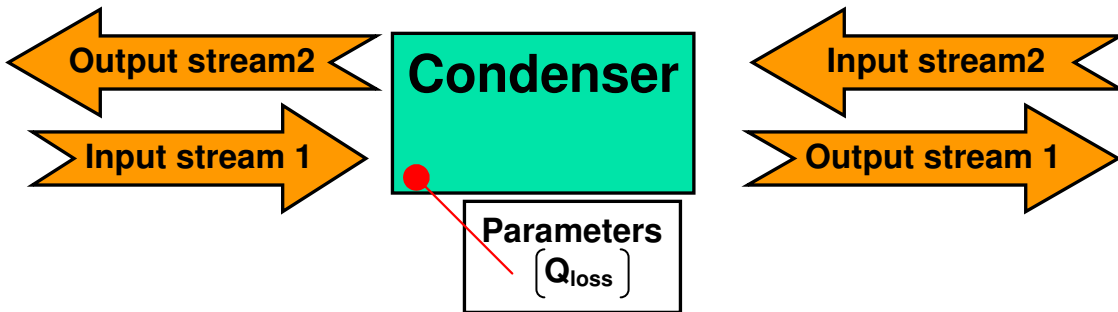
Figure 2.10 Condenser Element Model

Assumptions:

- Steam is condensed at constant pressure.

- Heat rejection occurs to the environment and is determined by an overall heat transfer coefficient h_c for heat transfer from the condenser to the environment and a surface area A_c. Both are assumed to be known.

$$\dot{Q}_c = -h_c A_c (T_1 - T_\infty)$$

- The surroundings are at known temperature T_∞ that is less than the saturation temperature of the mixture entering the condenser.

$$T_\infty \leq T_{sat}$$

- The fluid experiences negligible changes in kinetic and potential energy as it passes through the condenser.

$$V_1^2 - V_2^2 = 0$$
$$g(z_1 - z_2) = 0$$

- The subscripts 1 and 2 refer to properties measured at the component inlet and exit respectively.

Condenser Element:

Parameter	Symbol	Units
Heat Loss	Q_{loss}	kJ/kgK

Variables	Symbol	Units
None		

Constraints	Symbol	Value
None		

Governing Equations:

Ideal Gas Equation of State	$Pv = RT$	(2.9.1)
Specific Heat Equation	$dh = C_p(T)dT$	(2.9.2)
Gibbs Equation	$Tds = du + Pdv$	(2.9.3)
Conservation of mass	$\dot{w}_{in} = \dot{w}_{out}$	(2.9.4)
Energy	$\dot{E}_{in} = \dot{E}_{out}$ $$\dot{E} = \dot{Q} + \dot{W} + \sum m_i \dot{w}\left(h_i + \frac{V_i^2}{2} + gz_i \right)$$	(2.9.5)
Heat Transfer	$\dot{Q} = -A_c h_c (T_1 - T_2)$	(2.9.6)

Error Terms:

Term	Equation	Units
None		

Method of Solution:

Equation 2.9.6 is used to determine the net heat loss from the condenser to the environment. This is used as an input to CEA which, along with the input composition and temperature, solves equations 2.9.1-2.9.5 to find the output state and composition of the fluid exiting the system.

2.10 *Low Temperature Separator Element Model*

Schematic Diagram:
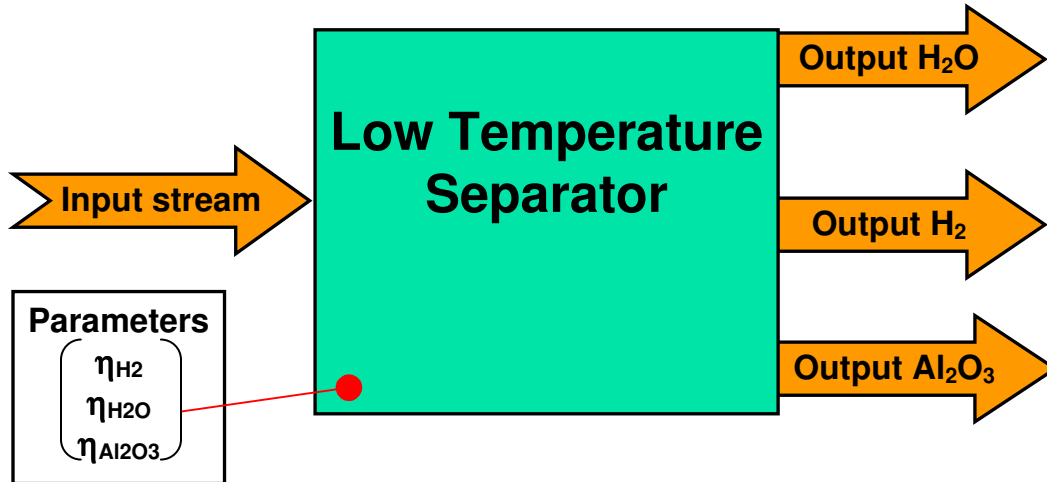
Figure 2.11 Low Temperature Separator Element Model

Assumptions:

- The total temperature T_0 and the mole fractions y_i of the inputs are known.

- The subscripts 1, 2 and 3 refer to properties measured at the component inlet, pure gas exit and liquid H_2O exit respectively.

- The subscript *i* refers to the individual species being considered. In this case, *i=1* corresponds to H_2O, *i=2* corresponds to H_2 and *i=3* corresponds to Al_2O_3.

- The amount of work required to separate a mixture into its pure components is equal to the ideal reversible work produced by mixing:

$$W_{rev} = -R_u T \sum_i^n N_i \ln y_i$$

- There is no work input to the separator, thus all work performed to separate the mixture comes from the input stream.

- The separation efficiency for each of the constituents is given by:

$$\eta_{Al} = \frac{\dot{w}_{Al,4}}{\dot{w}_{Al,1}} \qquad \eta_{H2O} = \frac{\dot{w}_{H2O,3}}{\dot{w}_{H2O,1}} \qquad \eta_{H2} = \frac{\dot{w}_{H2,2}}{\dot{w}_{H2,1}}$$

- The amount of alumina present in the separated H_2 and H_2O streams is negligible

- The amount of H_2 and H_2O present in the separated alumina stream is negligible.

- The separation process occurs adiabatically.

- The temperatures of the H_2 and H_2O streams exiting the separator are the same.

Low Temperature Separator Element:

Parameter	Symbol	Units
Separator H_2 efficiency	η_{LTS,H_2}	None
Separator H_2O efficiency	η_{LTS,H_2O}	None
Separator Al_2O_3 efficiency	η_{LTS,Al_2O_3}	None

Variable	Symbol	Units
None		

Constraints	Symbol	Value
None		

Governing Equations:

Ideal Gas Equation of State	$Pv = RT$	(2.10.1)
Conservation of mass	$\dot{w}_{in} = \dot{w}_{out}$	(2.10.2)
Conservation of Energy	$\dot{E}_{in} = \dot{E}_{out}$ $$E = \dot{Q} + \dot{W} + \sum m_i \dot{w}\left(h_i + \frac{V_i^2}{2} + gz_i \right)$$	(2.10.3)
Entropy	$$\Delta s = \int_{T_1}^{T_2} C_p \frac{dT}{T} - \int_{P_1}^{P_2} \left(\frac{\partial v}{\partial T} \right)_P dP$$	(2.10.4)

Error Terms:

Term	Equation	Units
None		

Method of Solution:

The process of mixing generates entropy. For a process involving n components, the entropy generated is given by [44]:

$$S_{gen} = -R_u \sum_i^n N_i \ln y_i \qquad (2.10.5)$$

The amount of work that is lost during a mixing process can be determined by the product of the entropy generated and the temperature of the surroundings in which mixing took place.

$$W_{lost} = T_{env} S_{gen} \qquad (2.10.6)$$

The separation process is a reversal of mixing. Therefore, the amount of work required to completely separate the components of a mixture into its components is, at least:

$$W_{separation} = -R_u T \sum_{i}^{n} \dot{N}_i \ln y_i \qquad (2.10.7)$$

where $i=1$ corresponds to Al_2O_3, $i=2$ corresponds to H_2O, and $i=3$ corresponds to H_2. Re-writing 2.10.7 in terms of the weight flow and the molecular weight of species i, MW_i gives:

$$\dot{W}_{separation} = -R_u T \sum_{i=1}^{3} \frac{\dot{w}_{i,1}}{g} MW_i \ln y_{i,1} \qquad (2.10.8)$$

Conservation of mass is used to determine the weight flow rates of the individual species exiting the control volume through the four discharges (gas-phase and solid-phase). The mass of the alumina in the gas and liquid streams is assumed to be negligible, so:

$$\dot{w}_2 \cong \eta_{H2} \dot{w}_{H2,1} + (1 - \eta_{H2O}) \dot{w}_{H2O,1} \qquad (2.10.9)$$

$$\dot{w}_3 \cong (1 - \eta_{H2}) \dot{w}_{H2,1} + \eta_{H2O} \dot{w}_{H2O,1} \qquad (2.10.10)$$

$$\dot{w}_4 = \eta_{Al2O3} \dot{w}_{Al2O3,1} \qquad (2.10.11)$$

Note that the amount of H_2 and H_2O captured in the alumina filter is assumed to be zero and that the amount of alumina in the H_2 and H_2O streams is taken to be zero. The mole fractions in the outlet streams are determined from the flow rates of the individual species.

$$y_{i,2} = \frac{\dfrac{w_{i,2}}{g} MW_i}{\sum_{i=1}^{3} \dfrac{w_{i,2}}{g} MW_i} \qquad y_{i,3} = \frac{\dfrac{w_{i,3}}{g} MW_i}{\sum_{i=1}^{3} \dfrac{w_{i,3}}{g} MW_i} \qquad y_{i,4} = \frac{\dfrac{w_{i,4}}{g} MW_i}{\sum_{i=1}^{3} \dfrac{w_{i,4}}{g} MW_i} \qquad (2.10.12\text{-}14)$$

59

The output enthalpy is determined using conservation of energy for an adiabatic process.

$$\sum_{i=1}^{3} mf_{i,1}\dot{w}_1 h_{i,1} = \dot{W}_{separation} + \sum_{i=1}^{3} mf_{i,2}\dot{w}_2 h_{i,2} + \sum_{i=1}^{3} mf_{i,3}\dot{w}_3 h_{i,3} + \sum_{i=1}^{3} mf_{i,4}\dot{w}_4 h_{i,4} \qquad (2.10.15)$$

The total system enthalpy is a mass weighted average of the individual component enthalpies at the temperature and pressure of the mixture. Therefore, the temperatures of the components exiting the separator decrease in order to compensate for the separation enthalpy. Two assumptions are necessary to find the temperatures of the streams exiting the separator. The first is that the last term in 2.10.15 is negligible with respect to the others. The second is that temperatures of the water and hydrogen streams are the same. Therefore:

$$\sum_{i=1}^{3} mf_{i,1}\dot{w}_1 h_{i,1} \cong \dot{W}_{separation} + \sum_{i=1}^{3} mf_{i,2}\dot{w}_2 h_{i,2} + \sum_{i=1}^{3} mf_{i,3}\dot{w}_3 h_{i,3} \qquad (2.10.16)$$

And:

$$T_{i,2} = T_{i,3} \qquad (2.10.17)$$

Rearranging 2.9.16 to solve for the loss in enthalpy, and introduce a new parameter α, which will enable an iterative solution:

$$\alpha = \frac{\Delta h_{H_2O}}{\dot{W}_{separation}} \qquad (2.10.18)$$

$\alpha = 1$ implies that all of the work of separation is from a loss in enthalpy of the water, and a $\alpha = 0$ implies that all the work of separation is from a loss in enthalpy of the hydrogen. The output states can then be individually computed based on a guess of phi.

$$mf_{H_2,2}\dot{w}_2 h_{H_2,1} - (1-\alpha)\dot{W}_{separation} = mf_{H_2,2}\dot{w}_2 h_{H_2,2} \qquad (2.10.19)$$

60

$$mf_{H_2O,2}\dot{w}_2 h_{H_2O,1} - \alpha\dot{W}_{separation} = mf_{H_2O,2}\dot{w}_2 h_{H_2O,2} \tag{2.10.20}$$

Assuming ideal gas behaviors for high temperatures and relatively low pressures:

$$T_{H_2,2} = \frac{mf_{H_2,2}\dot{w}_2 Cp_{H_2}T_1 - (1-\alpha)\dot{W}_{separation}}{mf_{H_2,2}\dot{w}_2 Cp_{H_2}} \tag{2.10.21}$$

$$T_{H_2O,2} = \frac{mf_{H_2O,2}\dot{w}_2 Cp_{H_2O}T_1 - \alpha\dot{W}_{separation}}{mf_{H_2O,2}\dot{w}_2 Cp_{H_2O}} \tag{2.10.22}$$

The true solution will be the α value for which the temperatures of both components are equal.

61

2.11 *Pump/Compressor Element Model*

Schematic Diagram:
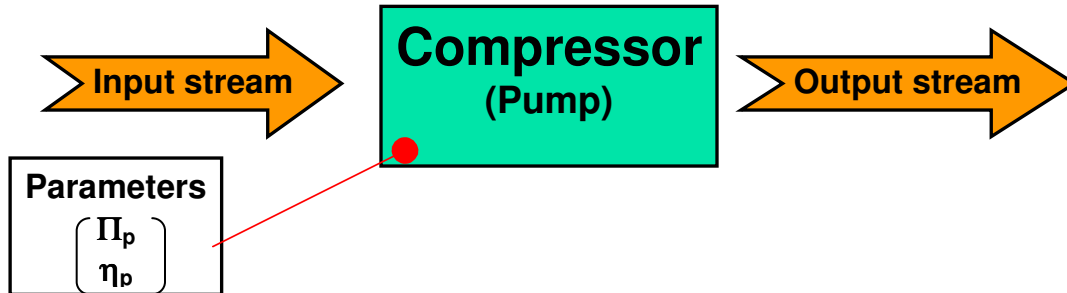
Figure 2.12 Pump/Compressor Element Model

Assumptions:

- All inputs are assumed to be entering at temperature T_1 and pressure P_1. The

  thermodynamic state of the liquid is determined from two intrinsic properties:

$$h = f_1(T_1, P_1)$$
$$s = f_2(T_1, P_1)$$

- Performance depends only on the pressure ratio, Π_P and the isentropic efficiency,

  η_P.

$$\Pi_P = \frac{P_2}{P_1} \qquad \eta_P = \frac{h_{2s} - h_1}{h_2 - h_1} = \frac{W_{ideal}}{W_{actual}}$$

- There are no viscous losses and no heat loss due to conduction through the walls

  (adiabatic).

$$\dot{Q}_{loss} = 0$$

- The fluid experiences negligible changes in kinetic and potential energy as it

  passes through the element.

$$V_1^2 - V_2^2 = 0 \qquad g(z_1 - z_2) = 0$$

- The subscripts 1 and 2 refer to properties measured at the component inlet and exit respectively.

Pump/Compressor Component:

Parameter	Symbol	Units
Pressure Ratio	Π_P	None
Isentropic efficiency	η_P	None

Variable	Symbol	Units
None		

Constraints	Symbol	Value
None		

Governing Equations:

Conservation of mass	$\dot{w}_{in} = \dot{w}_{out}$	(2.11.1)
Conservation of Energy (Rate Form)	$\dot{E}_{in} = \dot{E}_{out}$ $\dot{E} = \dot{Q} + \dot{W} + \sum m_i \dot{w} \left(h_i + \dfrac{V_i^2}{2} + gz_i \right)$	(2.11.2)
Enthalpy	$\Delta h = \int\limits_{T_1}^{T_2} C_p dT + \int\limits_{P_1}^{P_2} \left[v - T \left(\dfrac{\partial v}{\partial T} \right)_P \right] dP$	(2.11.3)

| Entropy | $$\Delta s = \int_{T_1}^{T_2} C_p \frac{dT}{T} - \int_{P_1}^{P_2} \left(\frac{\partial v}{\partial T} \right)_P dP$$ | (2.11.4) |

Error Terms:

Term	Equation	Units
None		

Method of Solution:

Output Pressure:

From conservation of energy (2.11.2) the shaft work input raises the enthalpy of the constituent mixture by:

$$\frac{\dot{w}_1}{g} h_1 + \dot{W} = \frac{\dot{w}_2}{g} h_2 \qquad (2.11.5)$$

h_1 is the enthalpy per unit mass of the inlet mixture, which can be determined using the initial temperature, pressure, and equation 2.11.3. However, performing this integration for each temperature change is computationally inefficient. Instead, lookup tables of enthalpy as a function of temperature and pressure are generated ahead of time for use in the calculations. NPSS generates this table by calling CEA, one of its standard thermodynamics packages.

The following NPSS commands are used to retrieve the enthalpy and entropy of the inlet composition from the database:

$$Fl.I.setTotal\_TP(T_1, P_1) \qquad (2.11.6)$$

$$h_1 = Fl.I.ht \qquad (2.11.7)$$

$$s_1 = Fl.I.S \tag{2.11.8}$$

The exit pressure is determined using the pressure ratio:

$$P_2 = \Pi_p \times P_1 \tag{2.11.9}$$

Since no reactions are taking place, conservation of mass (2.11.1) requires that the water entering the element have the same species fraction as the water leaving. This enables one to temporarily "copy" the entrance flow to the exit:

$$Fl.O.copyFlow("Fl.I") \tag{2.11.10}$$

The state at the outlet under an ideal (i.e. isentropic compression) process is determined by setting the state using the exit pressure P_2 and the entrance enthalpy s_1

$$Fl.O.setTotalSP(s_1, P_2) \tag{2.11.11}$$

then by referencing the enthalpy of the fluid at this state:

$$h_{2s} = Fl.O.ht \tag{2.11.12}$$

the actual enthalpy at the exit, h_2, can be computed using the definition of the isentropic efficiency presented in the assumptions section:

$$h_2 = h_1 + \frac{(h_{2s} - h_1)}{\eta_p} \tag{2.11.13}$$

Substituting the results of the calculations in 2.11.13, and 2.11.7 into 2.11.5 enables one to solve for the power:

$$\dot{W}_{in} = \dot{w}(h_2 - h_1) \tag{2.11.14}$$

NPSS uses this required power as a parameter:

$$Sh.I.pwr = \dot{W}_{in} \tag{2.11.15}$$

NPSS automatically solves for a shaft power balance between the turbine output power and the required input powers of all the components as it converges on a solution to the system.

Finally the conditions at the outlet are specified using fluid property package based on the pressure and enthalpy:

$$Fl.O.setTotal\_hP(h_2, P_2) \qquad (2.11.16)$$

2.12 *Splitter Element Model*

Schematic Diagram:
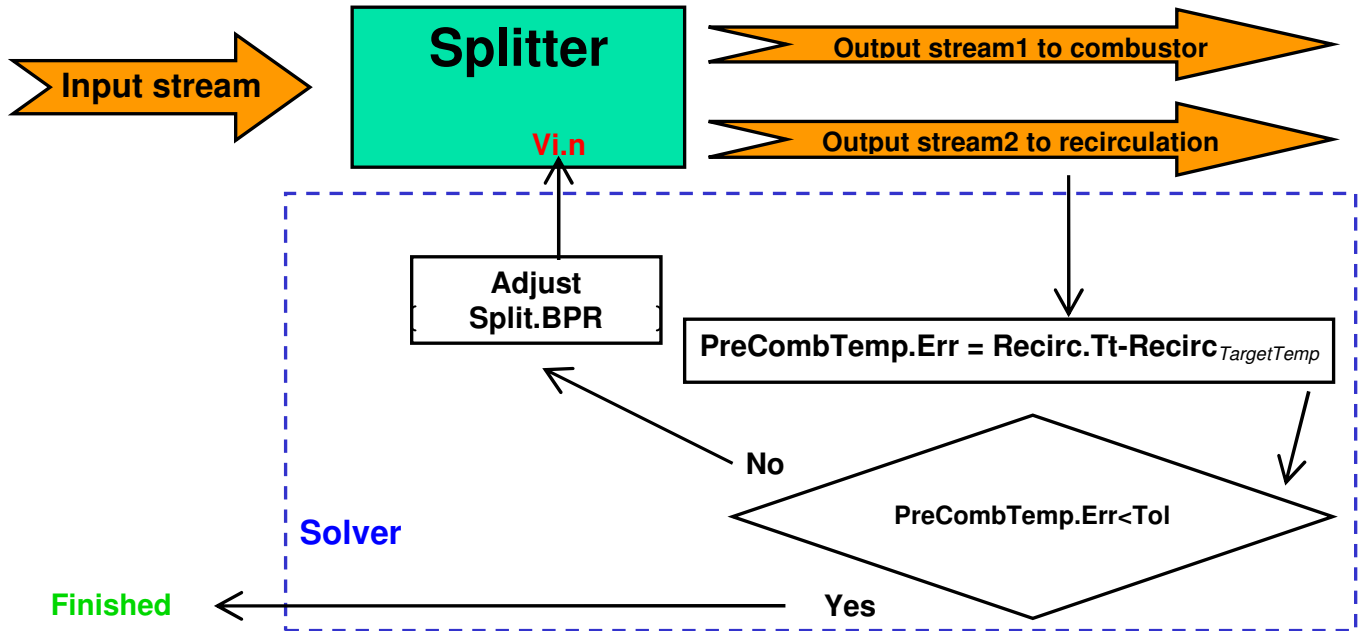
Figure 2.13 Splitter Element Model

Assumptions:

- Input comes from one source, and leaves as two flow streams.

- The thermodynamic state is determined from two intrinsic properties. Others can

  be calculated through functional relationships or using lookup tables:

$$h = f_1(T_1, P_1)$$
$$s = f_2(T_1, P_1)$$

- There are no viscous losses in the mixer and no heat loss due to conduction

  through the walls (adiabatic).

$$\dot{Q}_{loss} = 0$$

- The fluid experiences negligible changes in kinetic and potential energy as it undergoes mixing.

$$V_1^2 - V_3^2 = 0$$
$$V_1^2 - V_2^2 = 0$$
$$g(z_1 - z_3) = 0$$
$$g(z_1 - z_2) = 0$$

- The subscripts 1, (2 = 3) refer to properties measured at the component inlet and exits respectively.

Splitter Element:

Parameter	Symbol	Units
None		

Variable	Symbol	Units
Splitter Bypass	*BPR*	None

Constraints	Symbol	Value
None		

Governing Equations:

Ideal Gas Equation of State	$Pv = RT$	(2.12.1)
Conservation of mass	$\dot{w}_{in} = \dot{w}_{out}$	(2.12.2)
Conservation of Energy	$\dot{E}_{in} = \dot{E}_{out}$	(2.12.3)

$$ \dot{E} = \dot{Q} + \dot{W} + \sum m_i \dot{w} \left(h_i + \frac{V_i^2}{2} + gz_i \right) $$

Error Terms:

Term	Equation	Units
Re-circulated Temperature	$\mathrm{Re}\,circ.Fl\_O.Tt - \mathrm{Re}\,circ_{T\arg et}.T$	Fahrenheit

Method of Solution:

The mixing process is a simple equilibrium calculation. Given the input states 1 and 2,

the output state will be homogeneous and the mixture enthalpy determined using NPSS.

The following NPSS commands are used to retrieve the enthalpy and entropy of the ith

inlet composition from the database:

$$ Fl\_I.setTotal\_TP(T_i, P_i) \tag{2.12.4} $$

$$ h_i = Fl.I.ht \tag{2.12.5} $$

$$ s_i = Fl.I.S \tag{2.12.6} $$

NPSS uses the conservation of energy(2.12.3) for an adiabatic process:

$$ \begin{aligned} \dot{w}_1 h_1 + \dot{w}_2 h_2 &= \dot{w}_3 h_3 \\ \dot{w}_1 (h_3 - h_1) &= \dot{w}_2 (h_2 - h_3) \end{aligned} \tag{2.12.7} $$

The final temperature, T_3, of the mixture can be determined since the enthalpy (2.12.7)

lost by one stream equals the entropy gain of the other. The final state of the mixture will

be determined at the exit temperature calculated above, but using the change in entropy to

set the state.

$$Fl.O.setTotalSP(s_1 + s_2 + S_{gen}, T_3) \qquad (2.12.8)$$

Chapter 3. Model Solution, Convergence, and Validation

3.1 Modeling

3.1.1 Multi-Degree of Freedom System Challenges

Developing thermodynamic models for the individual components summarized in Chapter 2 is relatively straightforward. However, solving the system of coupled components presents a number of challenges. For instance, the typical 'state space' representation of the system requires at least nine states (mass flow of hydrogen/water/aluminum, pressure, density, temperature, water quality, enthalpy, and entropy).   More could be required if the pressure, density, temperature, entropy or enthalpy are broken down into component contributions. This system could be solved by treating each component as a matrix that operates on the incoming state space vector. However, this approach becomes considerably more difficult as the number of components in the system grows and problems with sparse and nearly singular matrices will inevitably arise.

3.1.2 NPSS Advantages

NPSS was chosen to perform the system integration in order to avoid the need to write our own code that would implement solutions to the difficulties mentioned above. One advantage of NPSS is that it can handle large system simulations and comes packaged with steady state and transient system solvers. Another advantage of NPSS is that it uses thermodynamic modules of varying complexity to simulate all of the components of a turbojet engine, and these elements, like compressors and turbines, are applicable to a

wide range of thermodynamic cycles. Thus many of the elements needed to simulate the Rankine cycle can be pulled of the 'NPSS shelf' almost ready to go. The NPSS Developers Guide is a useful tool for modifying these components. Also, NPSS is built and compiled using a C++ architecture. This is more computationally efficient than simulations run in environments like Matlab (or similar) [41].

3.1.3   Assembling the Model

NPSS uses a state vector element to hold all of the flow properties mentioned in the introduction, however, it stores them in a C++ element called a structure. The benefit of this method is that each parameter can be called or referenced independent of the others. Thus each component model is no longer represented as a matrix. Instead, the model elements are simply expressed as a series of equations relating specific inputs to specific outputs.

Once a component model has been created, it is stored individually as an 'interpreted component.' Including interpreted components in a model is as simple as listing the name of the element and initializing its parameter values.

The model is assembled in NPSS by listing each element sequentially in the order in which the system will be solved. Once all the component models are listed, they are connected in the NPSS architecture by linking 'Flow Ports' corresponding to the input and output streams. Flow ports are references which tell NPSS that the output from element A becomes the input to element B.

The Al combustion system model is solved in the following order. The numbers in parentheses correspond to the sub-section number of Chapter 2 where the element is described.

1. Hydrogen Fuel Start (2.2)

   a. Parameter: Mass Flow, Temperature, Pressure

2. Aluminum Seeder (2.3)

   a. Parameter: Seeding value, Pressure Loss, Temperature

3. Recirculation from combustion(guess) (2.4)

   a. Variable: Mass flow, Temperature, Pressure

   b. Dependant: Mass flow, Temperature, Pressure

4. Flow Start of Ambient Water (2.2)

   a. Parameter: Mass flow, Temperature, Pressure

5. Turbine output (guess)(2.6)

   a. Variable: Mass flow, Temperature, Pressure

   b. Dependant: Mass flow, Temperature, Pressure

6. Heat Exchanger (2.7)

   a. Variable: Effectiveness

   b. Dependant: Quenching Water Temperature

7. Flow Splitter (2.12)

   a. Variable: Splitting Ratio

   b. Dependant: Recirculation Water Temperature

8. Pre-Combustor and Quenching (2.5)

   a. Sub-Solver: CEA

   b. Parameter: Pressure Loss

9. Separation (2.7)

   a. Variable: Bypass Ratio

b. Dependant: Recirculation Mass Flow

c. Parameter: Separation efficiency, Pressure loss

10. Recirculation Quenching(2.5)

a. Sub-Solver: CEA

11. Recirculation Compression (2.11)

a. Parameter: Pressure Ratio, Efficiency

This is the end of the recirculation loop. Data is compared to the initial guess at step 3 for

convergence. Then the solution moves on to the turbine output

12. Turbine (2.8)

a. Parameter: Pressure Ratio, Efficiency

Again the values here are checked against the approximations made in step 5.

13. Condensing(2.9)

a. Parameter: Net heat extracted

14. Low Temp Separator(2.10)

a. Parameter: Separation efficiency

3.2 *NPSS Solution Methods*

Before a solution can be generated, the components must be linked using the simple

command, linkports(x1,x2,n), which takes inputs x1and x2 which are flow port types and

'n' the name of the linkage. See the appendix, or the Dev. Guide[42] for examples. Once

the components of the system have been successfully linked, the system is passed to the

NPSS solver. The solver identifies the independent and dependent variables and performs

a series of perturbations to calculate a numerical approximation to the Jacobian matrix,

which is a matrix of partial derivatives that relates the independent variables to the

dependent reference conditions. A modified Newton Rhapson method uses the Jacobian matrix to 'step' in the direction of decreasing error. NPSS adaptively changes the step size based on the previous reduction in error in order to increase computational efficiency. New Jacobians are not necessarily computed at every new location as this would be computationally expensive. Instead, they are computed on an 'as needed' basis when the residual fails to decrease adequately between iteration steps.

One of the challenges associated with using NPSS is that it requires that there be an equal number of dependent and independent variables. Of course, systems often have more independent conditions than dependent ones. Therefore, some system variables must be parameterized and only varied by the user outside the system solver. An example in this work is the fuel mass flow.

To reiterate from Chapter 2, three independent variables were chosen to describe the system: the separator and splitter bypass ratios and the regenerator effectiveness. Six more variables were introduced to account for the recirculation present in the system but do not have any true analog in the physical system. However, the three independent variables do. The separator bypass ratio is the ratio of fluid passed back to continue the combustion process to the fluid which goes on to the turbine. The splitting ratio is the ratio of the mass flow of fluid which enters the recirculation leg to the mass flow which directly quenches the combustion products. Finally, the variable regenerator effectiveness can be thought of as simply the level of regenerator performance which is required to produce re-heated water at the specified state point regardless of the turbine exit temperature and mass flow.

3.3 *Input Variation*

The NPSS model was run at two different sets of state points based on information contained in two references provided by NUWC [39,40]. Again, these tables of target values are listed in the appendix. The differences shown between the Case 1 and Case 2 predictions stem at least in part from the fact that each calculation is based on slightly different assumptions and constraints. The state points and associated assumptions for both cases are shown in Table 3.2. The differences between the two cases are discussed in the following sections. Note that in almost every instance, Case 1 makes more pessimistic assumptions than Case 2 in terms of operational temperature, pressure losses through the system and required mass flow.

	Case 1 [39]	Case 2 [40]	Units
Target Changes			
Recirculation Temperature			
Recirculation Mass Flow			
Quenching Water Temp			
Parameter Changes			
Aluminum mass flow			
Turbine efficiency			
Seeder pressure ratio			
Recuperator pressure ratio			
Condenser pressure ratio			
Separator temperature drop			
Feed water Temperature			

**Table 3.1 Differences in NPSS inputs for each simulation.**

For the two cases, the values of the interesting independent variables (from table 2.1) at convergence are listed in table 3.2. These values fix the 'geometry' of the engine.

	Separator Bypass	Splitting Ratio	Regenerator Eff.
Case 1			
Case 2			

Table 3.2 Values of independent variables at convergence.

3.4   *Demonstrating Convergence*

To establish that NPSS was actually converging on a 'real' solution, the system was started from several different values of the separator and splitter bypass ratios, *BPR* and β respectively, and allowed to converge while the temperature of the water entering the pre-combustor was monitored. Figure 3.1 shows that NPSS converges quickly to the same solution when 'good' guesses for β and *BPR* are made.
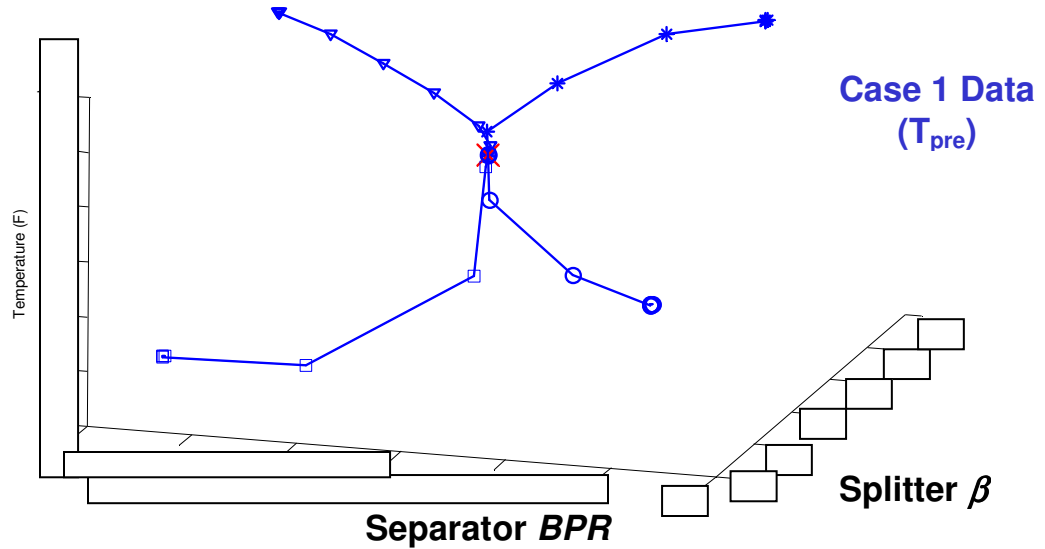
Figure 3.1 Demonstrating 'Open Ball' Convergence

This behavior is typical of Newton methods that are guaranteed to converge as long as the initial guess is sufficiently close to the true solution. Figure 3.1 shows that the state points for Case 1 lie within the convergence 'radius' for the NPSS system model. However, the Case 2 state points do not. As a result, some small modifications to the Case 2 state points were required in order to get the system to converge. In particular, the mass flow rate of the quenching water stream needed to be reduced by approximately 3%. Without this change, it was not thermodynamically possible to meet the combustor outlet temperature target of [   ]F (see appendix). In the non-converging case, producing a plot of the convergence history like figure 3.1 is nearly unreadable as the predicted values make large leaps from one convergence step to the next.

3.5   *State Point Comparison*

The following set of figures compares two operating points computed by NPSS. The solid bars correspond to NPSS predictions. In the figures, blue corresponds to Case 1 while red corresponds to Case 2.

3.5.1 State Point Temperatures
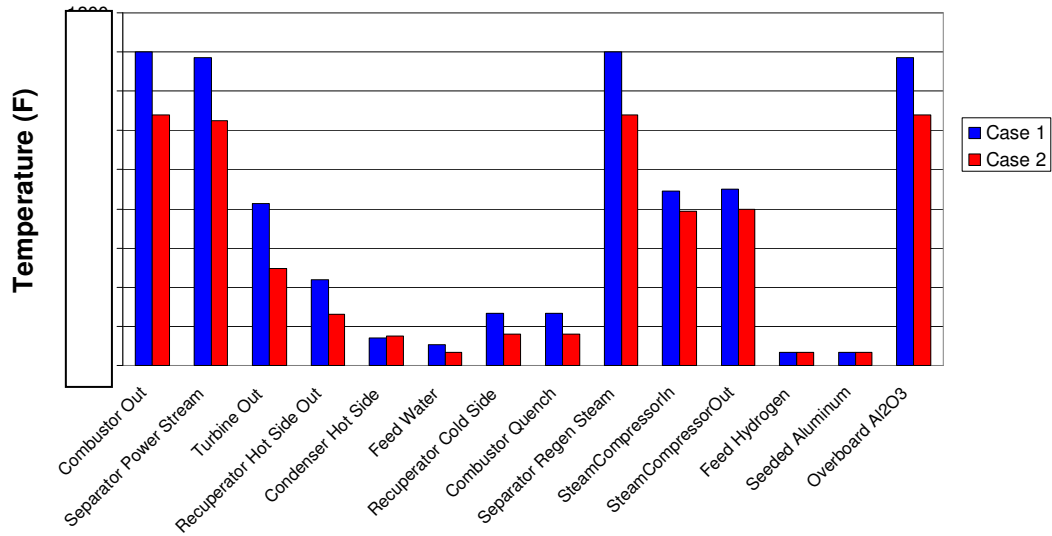
Figure 3.2 Comparison of state point temperatures.

Figure 3.2 shows temperature estimates at various points in the system for the two models. The most important difference is the combustor output temperature as the hot side temperature drives the overall performance of the cycle. It is higher in Case 1 primarily because of the increased mass flow rate and the increase in recirculation temperature. Another notable difference is the combustion quenching stream temperature, which is a function of regenerator effectiveness and the temperature at the turbine exit. This is higher in Case 1 because of the higher combustion temperature.

3.5.2 State Point Pressures
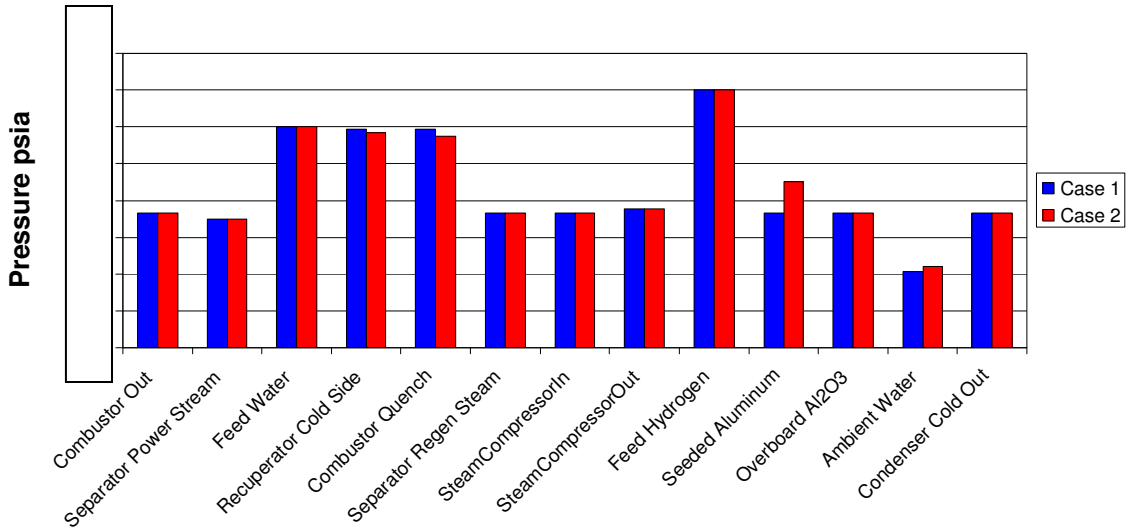
**Figure 3.3 Comparison of state point pressures.**

Figure 3.3 shows that the pressure differences between the predicted state points are very small and lie within the limits of numerical approximation. Since the model uses the state points to determine the pressure losses through components, this is more an indication that the model is working correctly computationally than an indication that the correct physics has been incorporated within the components. Further work would be required to incorporate the momentum equation into each element so that the mass flow through each component is actually driven by the pressure difference. This functionality would require a much more detailed analysis that incorporates the geometry of each component. Unfortunately, this sort of detailed information was not available. Finally, note that overboard Al_2O_3 pressure will limit the operational depth of the vehicle should exhausting Al_2O_3 overboard be required.

3.5.3   State Point Mass Flows
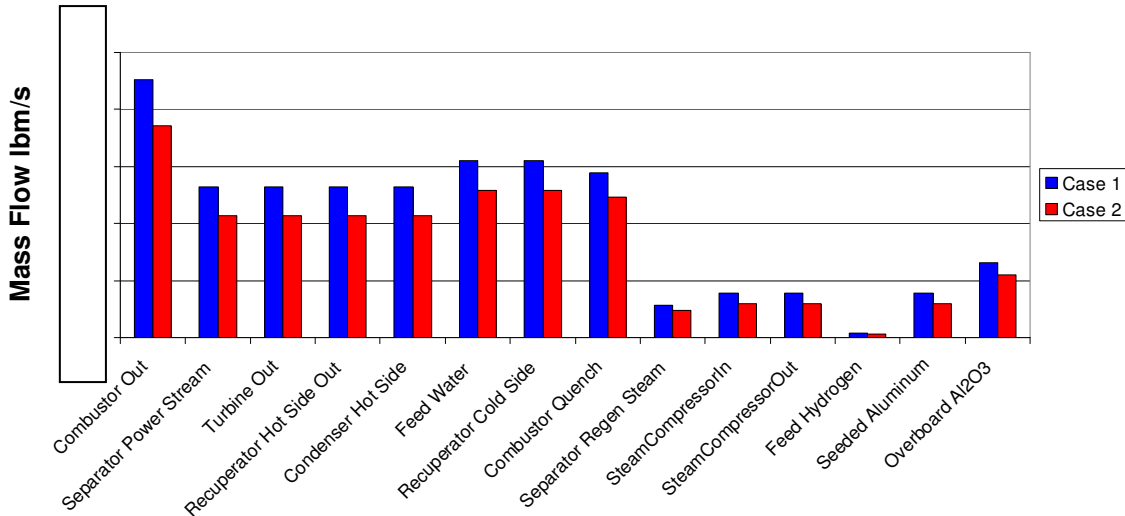
Figure 3.4 Comparison of Case 1, and Case 2 state point mass flow rates.

Figure 3.4 shows that there are several significant differences in the mass flow rates between cases 1 and 2.   This results from the fact that that the Case 1 and Case 2 analyses take fundamentally different approaches. Case 1 arbitrarily attempts to fix the shaft output power at the design value of ☐ Hp and then works backwards through the cycle to find the flow rates of water and aluminum that are required. Since Case 1 assumes that the turbine is significantly less efficient than Case 2 (☐ vs. ☐), more fuel is required and this, in turn, means that overall flow rates are larger. Table 3.3 shows that most of the differences between the Case 1 and Case 2 power outputs and mass flow rates can be attributed to the differences in assumed turbine efficiency. Note that since power is proportional to turbine efficiency and required mass flow is inversely proportional to the turbine efficiency, the ratios of power and turbine efficiency are compared to the inverse ratio of the mass flows.

	Power (Hp)	Comb mass flow (lbm/s)	Turbine efficiency (%)
Case 1			
Case 2			
Ratio			

Table 3.3 Effect of assumed turbine efficiency on mass flow rates and power outputs

3.5.4   Performance Comparison
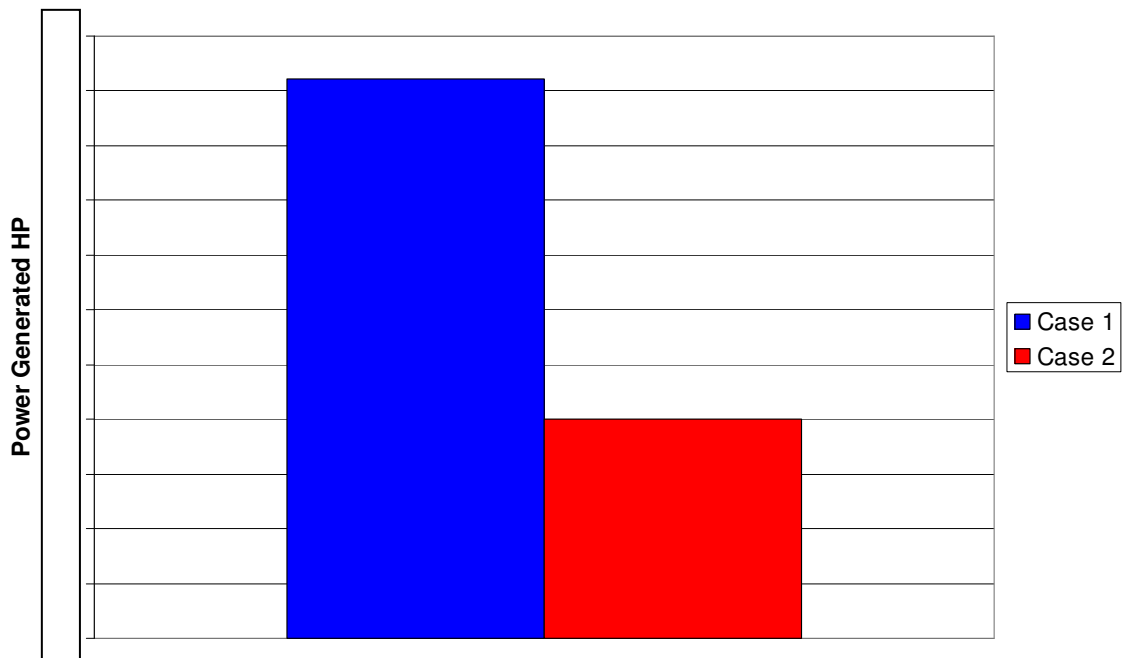
Figure 3.5 Power Output at Operating Points

Figure 3.5 compares the power output levels predicted by Case 1 and Case 2. The power output for Case 1 is higher as a direct result of the increase in mass flow. However a more interesting comparison, completed below, is the differences between these predictions and the references [39,40]. The last column of table 3.4 shows that after accounting for the differences in simplifying assumptions, and hence the relative

magnitude of the enthalpy, $\dot{m}C_p\Delta T$, the difference between [39,40] and NPSS power output predictions is negligible.

Consider case 1. The NPSS predicted power output is greater by a factor of 1/0.88. Ref 41 chose to ignore the hydrogen transport arguing its mass fraction was small and hence its effects were as well. However, the affect of hydrogen on the average value of C_p, even at small mass fractions (approximately 5%), is considerable because $C_{p,H2} \gg C_{p,steam}$. This is important because the power output of the turbine is given by:

$$P_{turb} = \dot{m}C_p T_{01}\eta_t\left[1-\left(P_{02}/P_{01}\right)^{\frac{\gamma-1}{\gamma}}\right] = \dot{m}C_p\eta_t\Delta T \,.$$

This is the primary driver in the difference between Case 1 and the predictions made by NPSS. In fact without any other mitigating causes, this would lead to the NPSS power output predictions being 125% of Case 2. However there is a second mitigating effect; the decreased mass flow NPSS predicts compared to Case 1. This is a result of an incorrect assumption made in Ref. 42 in the separator stage. Case 1 presumes that the separator only removes the mass of Al passed into the system. However, the true mass which must be removed is the mass of Al_2O_3. Including this oxide accounts for nearly 50% extra separation mass. Hence there is less mass flow available to the turbine in the NPSS simulation than in Case 1. Together these differences in starting assumptions account for 95% of the original discrepancy.

For Case 2 the situation is slightly more complex. Reference data for Case 2 suggests much higher (nearly a 1/3 more) power output available than predicted by the NPSS solution. To account for this discrepancy the turbine mass flow again comes under scrutiny. Examining Ref. 43 closely reveals that the system being modeled is not the entire power system. Instead, the pre-combustor is supplied by a separate high

temperature steam feed line. While this is the way combustion is sustained in the experiments reported in Ref 43, it is not the way combustion is sustained in the real system. As a result, the re-circulated mass flow calculated by NPSS required to sustain the reaction is never removed during the case 2 thermodynamic calculations. This decrease in mass flow for the NPSS simulation lowers the expected power output. The second factor which affects the case 2 simulation results is the significantly lower combustion temperature. In this case, combustion temperature changes of 100F are analogous to "data noise." For this reason, the Ref. 43 setup is running hotter than NPSS would predict for a single step reaction at the specified flow rates. These two contributions, mass flow and temperature, combined account for 95% of the discrepancy between 43 and NPSS. These results are very satisfying since they explain the difference among the data and predictions in a very succinct way.

	Power Output (Hp)	Efficiency (%)	Carnot efficiency (%)	C_p Steam @Tmax	C_p H_2 @Tmax	Mass Avg C_p	Turbine Flow (lbm/s)	Tmax (R)	ΔT Turbine (R)	$\dot{m}C_p\Delta T$
Case 1 [39] NPSS										
39/NPSS	0.88	0.88	0.99	1	0.997	0.753	1.142	0.97	1.027	0.83
Case 2 [40] NPSS										
40/NPSS	1.29	1.3	1.04	1.044	1.011	1.035	1.176	1.07	1.086	1.34

Table 3.4 Performance Comparison

3.5.5 Summary

Taken together, the results of these simulations indicate that from a basic thermodynamic viewpoint, the system is capable of producing at least ☐ Hp with at least ☐ % efficiency. This is significant because it suggests that a very substantial increase in range over conventional batteries is possible. Of course, the actual performance realized in practice will be lower due to additional losses in the system. The extent of this difference cannot

be determined without performing a much more detailed analysis that accounts properly for all significant losses in the system. Many of these losses will depend strongly on the details of the design. For example, one major contributor to pressure and thermal losses will certainly be the lengths, cross-sectional areas, and the types and numbers of bends in the tubes used to connect the various components together. All of these factors will need to be included to make more realistic predictions of system performance.

Chapter 4. Off Design Performance and System Sensitivity

4.1 *Off Design*

The NPSS model can also be used to explore the behavior of the system when it is operated off design, i.e. at operating conditions that are different from the single operating condition associated with the state points described in the previous Chapter. This is the model's main strength, as it enables system designers to study the effects of design changes in order to maximize system performance. Since NPSS can also study time-dependent problems, it can be used to predict transient performance. This capability will be very useful in studying the start up and shut down processes.

Table 4.1 shows the range of operating points that are explored for the Case 1 and Case 2 designs. The power output of the system is varied by increasing or decreasing the Al flow rate. This is accomplished easily in NPSS by slowly marching away from the state point solution by increasing or decreasing the mass flow of aluminum, using the most recently calculated solution as the guess, and then converging on a new solution. This method will work so long as large discontinuities are not present within the solution space.

	Case 1		Case 2	
	Power	BSFC/hr / % Eff	Power	BSFC/hr / % Eff
Model				
Max				
Min				
Units	Hp	lb/Hp-hr / %	Hp	lb/Hp-hr / %

Table 4.1 Available Performance Estimates

The model was run off design using two different techniques. The first 'fixed geometry' technique fixes the three variables, separator bypass, splitter ratio and heat exchanger effectiveness, to the converged values shown in table 3.1. This removes three dependent conditions used to specify the state point however, because NPSS can only run with an equal number of independent and dependent conditions. A new variable, the mass flow of quenching water into the system, is introduced to hold the temperature in the pre-combustor (the new dependant variable) constant while ensuring stoichiometric reaction in the pre-combustor. The model is run off design by increasing or decreasing the mass flow of aluminum and allowing this mass flow of the quenching water to similarly increase or decrease. This technique has the side affect of holding efficiency constant as it does not increase or decrease the ratio of re-circulated water, a primary driver of the efficiency.

The second off design run maintains all nine of the independent variables as independents. In this simulation, an increase in the mass flow of aluminum does not lead to an increase in the net water input to the system which is taken to be a fixed parameter.

The temperature in the pre-combustor must remain constant in order to ensure ignition, but unlike the previous case, the stoichiometry of the pre-combustor must be allowed to vary because the net water input to the system is fixed. In order to hold the temperature in the pre-combustor constant, all of the variables must change to account for the increasing combustion temperature and mass flow. This requires that more water be split off for combustion product quenching (BPR increases), while less water is bypassed from the separator (β decreases) as the temperature goes up. Since the mass flow rate of the quenching water does not increase at all, a limit is reached where the combustor no longer has enough water to react all of the Aluminum. Interestingly, under these conditions, a peak in efficiency is observed at slightly higher mass flow rates of aluminum than are used at the state point.

4.2 *Fixed Geometry Model Results*

The figure below shows the turbine power output as a function of aluminum mass flow rate. The original state point is labeled with a large star, and the solution is marched using a ☐ increment in the aluminum mass flow rate.
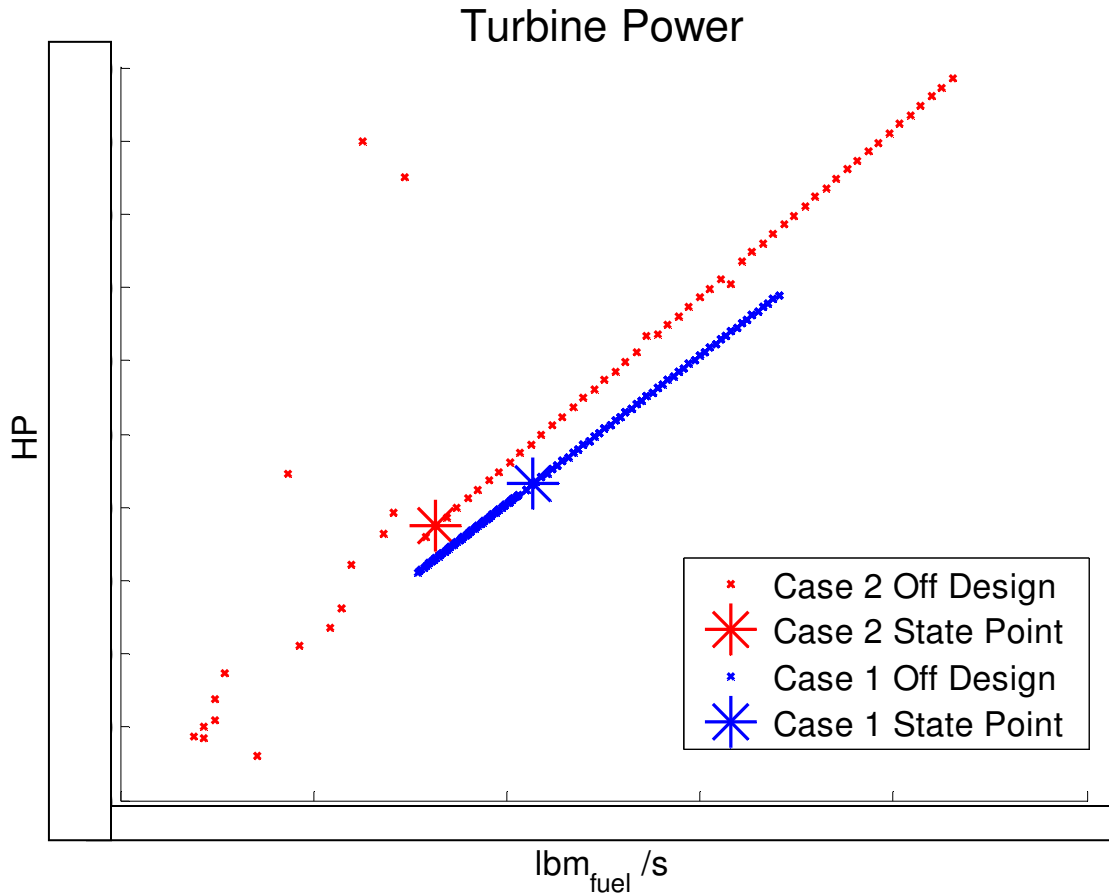

Figure 4.1 Computed turbine power output for both fixed geometry models

From figure 4.1 it is clear that the simulation results for the Case 2 conditions at fuel flow rates below 0 ☐ lbm/s show a large degree of uncontrolled variability. This is because the model has not converged and the values reported are simply those remaining in the model after 50 iterations, which is the default iteration limit in NPSS for solutions showing no signs of convergence.
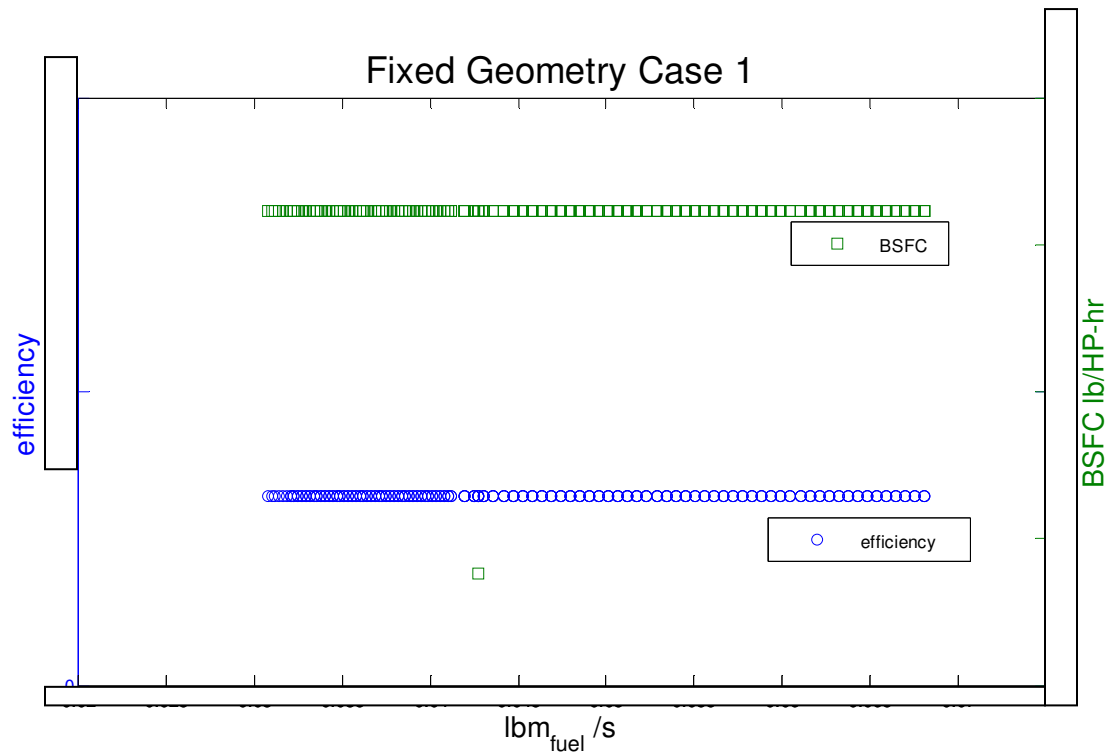
Figure 4.2 Efficiency and BSFC vs mass flow of fuel for fixed geometry model with Case 1 state point target

Figures 4.2 and 4.3 show the change in system efficiency as a function of fuel flow rate for the Case 1 and Case 2 specifications respectively. Efficiency is reported in two ways. The blue curves correspond to the thermodynamic efficiency defined as the power output divided by the power input via the chemical potential energy in the fuel. The green curves correspond to the Brake Specific Fuel Consumption (BSFC), which is a measure of the fuel mass required to produce a unit of energy (lb_{fuel}/ HP*hr). Therefore, high thermodynamic efficiency corresponds to low BSFC. Note that the efficiency does not change with fuel flow rate because of the fixed geometry assumption. The Case 1 system gives an overall efficiency of ___ % (BSFC= ___). The outlying data point in the Case 1 results does not correspond to a converged solution and should be disregarded.

90
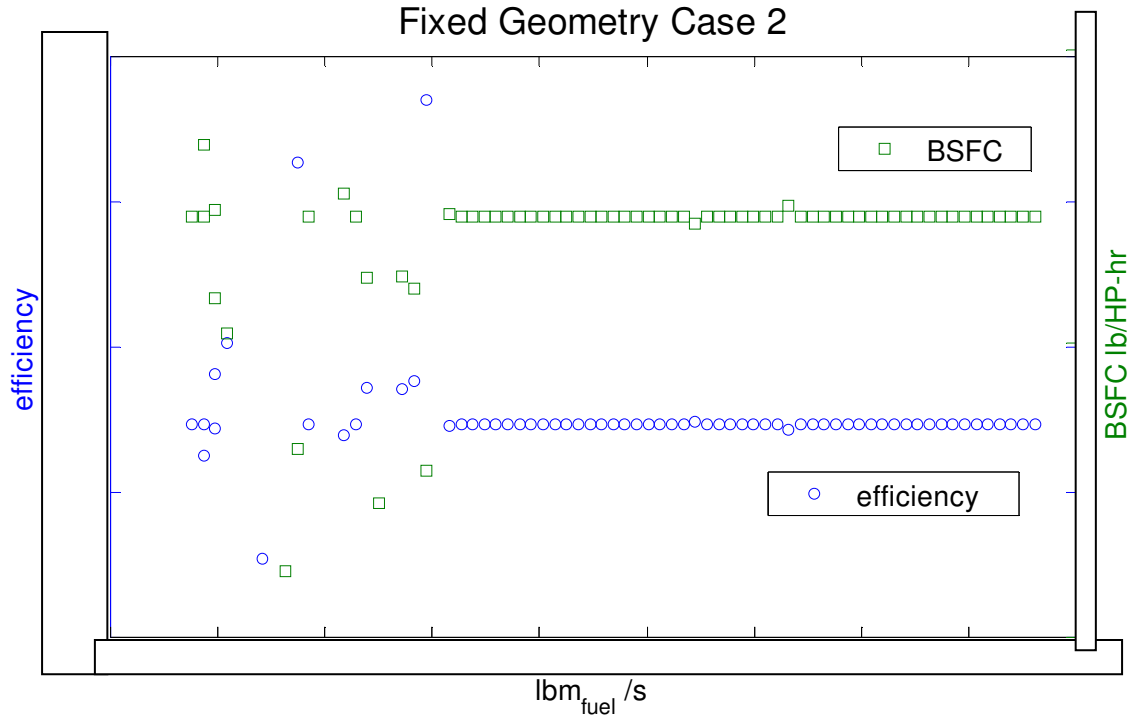
Figure 4.3 Efficiency and BSFC vs. mass flow of fuel for fixed geometry model with Case 2 state point targets

The convergence problems with the Case 2 system at low flow rates are apparent. When it does converge to a solution, the Case 2 system gives an overall efficiency of ☐ % (BSFC= ☐).

4.3 *Variable Geometry Model Results*
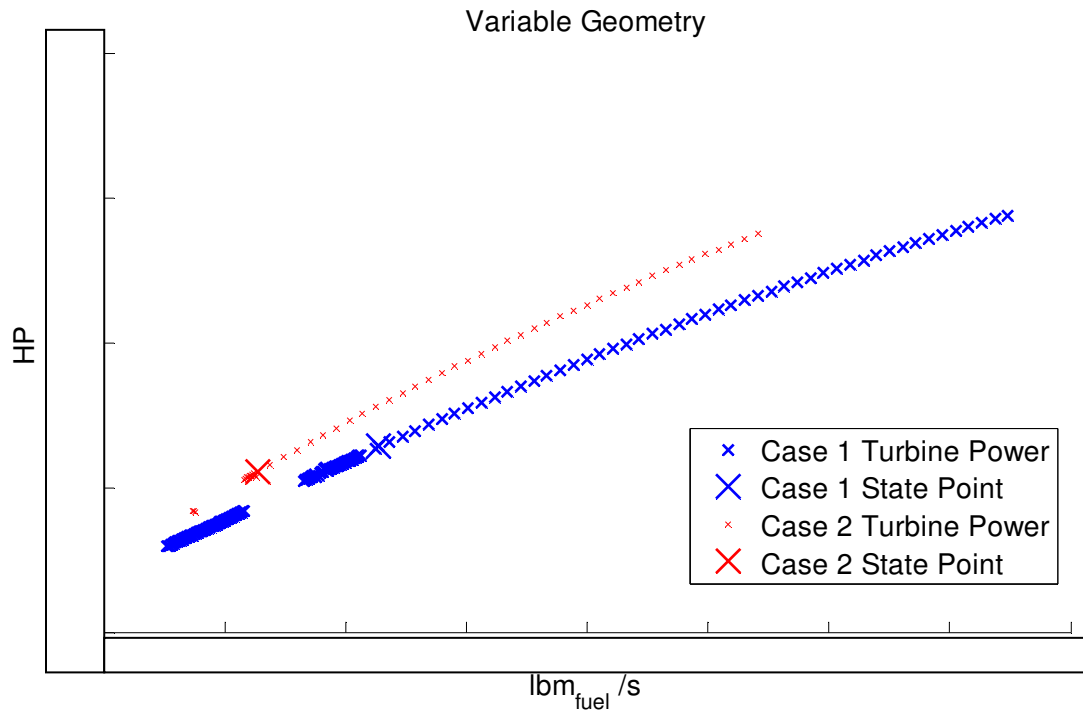
Figure 4.4 Computed turbine power output for both variable geometry models

Figure 4.4 shows the change in power output as the fuel flow is increased while the engine 'geometry' is allowed to vary. Note that this leads to a non-linear variation of power output with fuel flow rate. This non-linearity leads to a peak in efficiency at approximately ☐ HP as illustrated in figures 4.5 and 4.6. It also suggests that continued investigation might show that higher efficiencies than currently reported are available at lower mass flow rates for different system configurations.
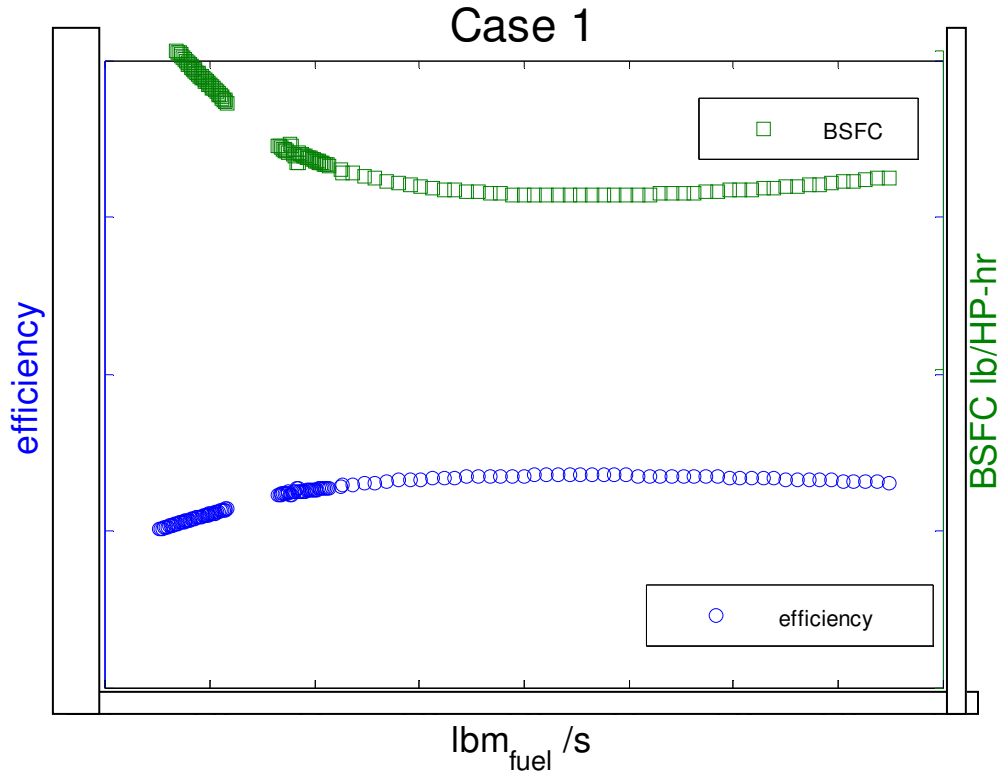
Figure 4.5 Efficiency and BSFC vs mass flow of fuel for variable geometry model with Case 1 state point targets

Figure 4.5 shows that for the Case 1 configuration, the peak efficiency of ____ % (BSFC =

_____) occurs at a slightly higher fuel mass flow of ____ lb/s corresponding to

the three dependent states (fixed mass flow, temperature of pre-combustion and

quenching water temperature). Once again, peak efficiency for Case 1 occurs at a power

output that is lower than the maximum value in the table.
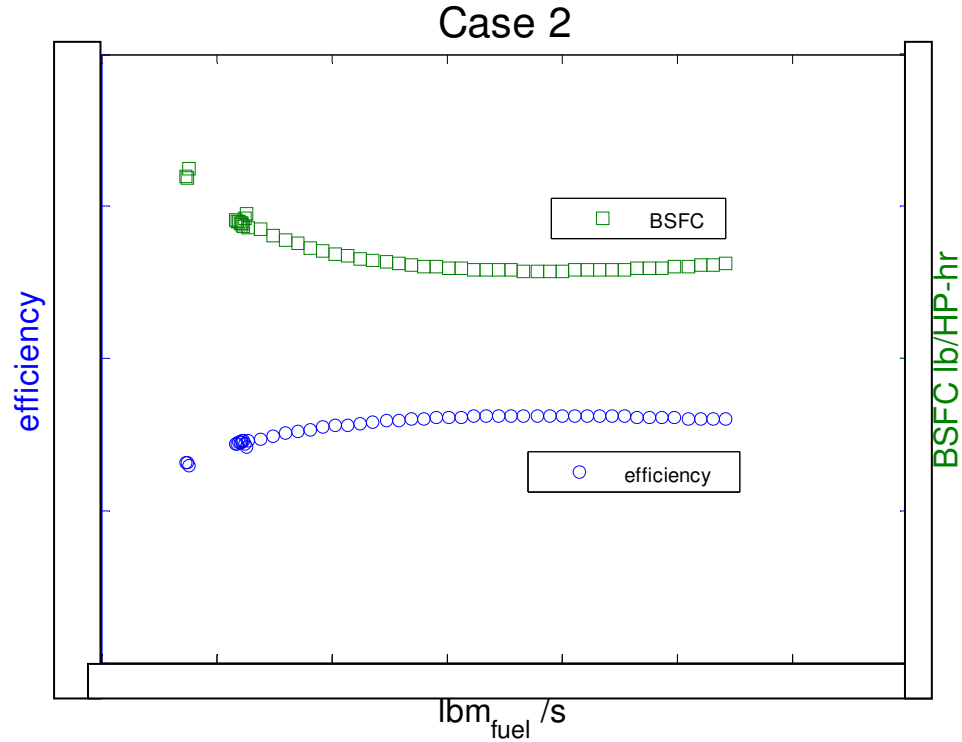
Figure 4.6 Efficiency and BSFC vs mass flow of fuel for variable geometry model with Case 2 state point targets

Figure 4.6 shows that for the Case 2 configuration, the peak efficiency of ☐ % (BSFC=☐) occurs at a fuel mass flow of (☐ lb/s corresponding to the three dependent states (fixed mass flow, temperature of pre-combustion and quenching water temperature). However, this does not correspond to the max power output in Table 4.1. Instead, it corresponds to ☐ HP which is lower than the peak of ☐ HP listed in the table.

4.4   *Preliminary Sensitivity Analysis*

Understanding the effects of design changes is very important for understanding how a system works as well as understanding how to make to make it better. Therefore, a very preliminary sensitivity analysis is presented in this section in order to provide some

94

insight into how changing certain design parameters influences the system's performance. Following this is a second analysis describing the effects of changing each of the three independent variables.
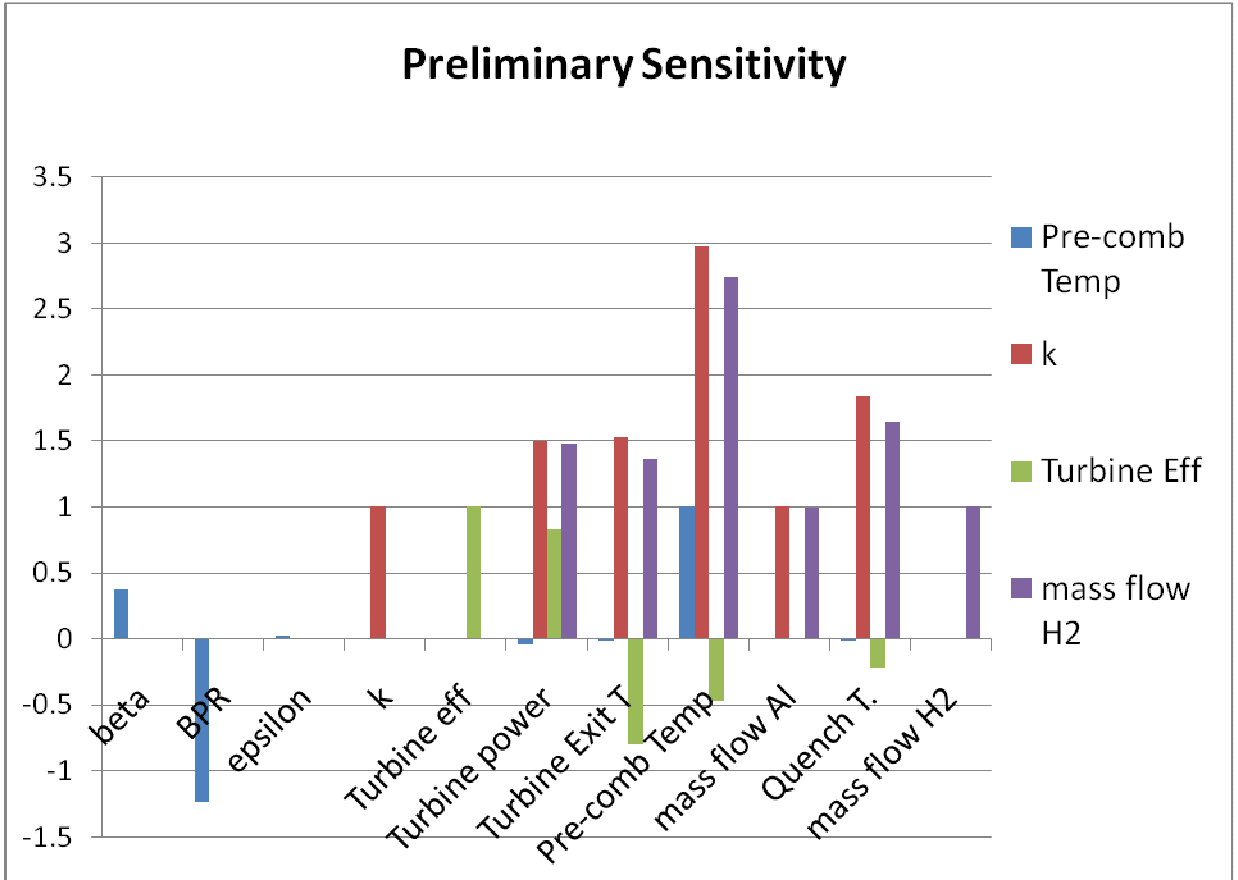
Figure 4.7 Case 1 based Parameter sensitivity

In this work, sensitivity is defined as the fractional change in the state point value divided by the fractional change in a parameter value. Mathematically this is written as:

$$S(\Delta PV) = \frac{\Delta s}{\Delta PV}$$

where S is the state point sensitivity being evaluated, Δs is the change in its value and ΔPV is the change in the parameter value. Rudimentarily speaking, this method generates a matrix of partial derivatives using single sided differencing to evaluate how steep the state space is. The sensitivities to four parameters are explored. These are the pre-

combustor temperature 'Pre-comb T', the seed capture efficiency 'seeding eff', the turbine efficiency 'Turbine Eff', and the mass flow of hydrogen 'mass flow H_2'. To perform the analysis, the model was run to convergence, one of four parameters was varied by 10%, and the solution was allowed to converge again.

Figure 4.7 shows the sensitivity of the system's state points to variations in the values of some of the parameters based on case 1 conditions. For example, figure 4.7 shows that the pre-combustor temperature is most sensitive to increases in 'seeding efficiency' (i.e. increasing the ratio of Al to H_2 in the fuel stream) and 'mass flow H_2'. It is not surprising that increasing either of these parameters increases the pre-combustor temperature. Increasing the turbine efficiency 'Turbine Eff', however, lowers the pre-combustor temperature because less waste heat is available to preheat the quenching water to achieve the same pre-combustor temperature. However, it is interesting to see that increasing the pre-combustor temperature independently of the other parameters actually yields a net decrease in turbine power. This is due to the increase in the amount of mass flow through the recirculation loop that is required to drive the pre-combustor temperature up. As with any combustion system, the limits on power output are the material temperature limits. The hotter the combustor can get, hence higher mass flow that can be used, the higher the turbine power output. Figure 4.7 demonstrates that there is a large amount of cross coupling between parameters, i.e. that small changes ($\sim\Delta10\%$) in one operating parameter can have a large impact ($\sim\Delta30\%$) on other operating parameters.
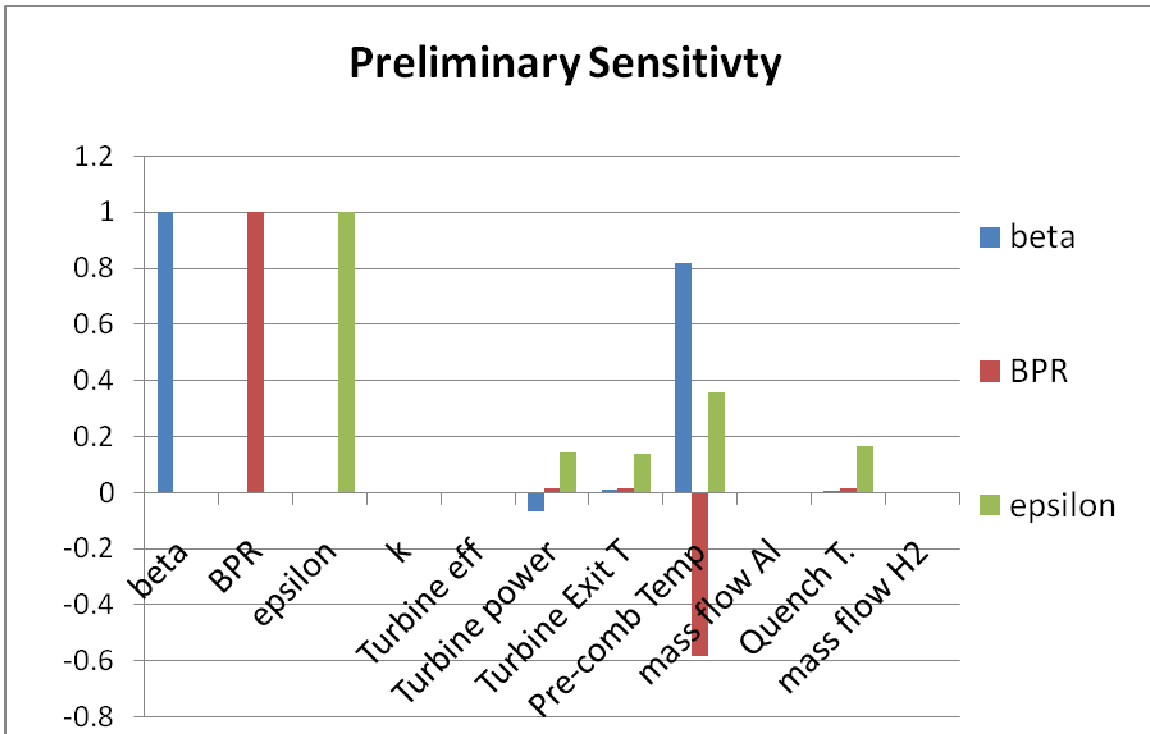
Figure 4.8 Independent variable sensitivity

Figure 4.8 shows the sensitivity of various state point conditions to changes in the independent variables manipulated in order to achieve convergence. Note that sensitivities of the state point values to changes in β, BPR, and ε are relatively small compared to the previous analysis. These reduced sensitivities show that the system is 'well behaved' in the region around the initial state point and explains why convergence is achieved rather easily using the Case 1 state points.

Chapter 5: Conclusion and Future Work

5.1   *Conclusion*

A numerical model of a novel Rankine Cycle underwater propulsion system based on the exothermic reaction of Aluminum powder with sea water has been developed. Elements of the system are modeled individually using simple thermodynamic models. These models are integrated using a system modeling tool called Numerical Propulsion System Solver (NPSS). The results indicate that the system should be capable of producing at least ☐Hp at an overall thermodynamic efficiency of ☐-☐% depending on the particular operating condition. While the performance of the actual system will undoubtedly be lower than the NPSS projections because of additional factors that are not included in the simulation like the particular geometry of the flow tubes, thermal losses to the environment, etc., the impact of these factors is expected to be relatively small and our results indicate that a factor of five improvement in the range of the Sea Horse UUV could be realized with this system.

While the NPSS results generally compare favorably to other simpler models of this system (Case 1 [39] and Case 2 [40]), there are differences that arise due to differences in the simplifying assumptions made by each modeler. In the Case 1 model, the prescribed mass flow of Al_2O_3 overboard was too low because the mass flow of oxygen overboard in the high temperature separator was neglected. Additionally, the effect of H_2 in the turbine was not accounted for but turns out to be important. After accounting for these differences, the NPSS calculations match the reference to within 5%. The Case 2 model used the wrong recirculation mass flow rate because it was based on an experiment that

used an auxiliary high temperature steam feed. Also, the combustion temperature used was different than what was calculated using CEA but insufficient information was provided in order to explain this discrepancy.   Again, however, adjusting the Case 2 NPSS results produces results that match the NPSS predictions to within 5%.   The reasons for this variation in combustion temperature are not clear because detailed information about what reaction mechanism, heats of formation, etc. was used to determine the combustion temperature in Case 2 was not available. Taken together, the NPSS approach not only appears to be sound but it has produced results that are more physically realistic than the previous two performance estimates.

A system sensitivity analysis showed that the power output, and hence efficiency, is most sensitive to mass flow, turbine efficiency and regenerator effectiveness. Therefore, efforts to improve the performance of the system should be focused in these areas. The regenerator effectiveness is especially important because in the confined space there is not much room available to accomplish this heat transfer task. The overall system design is most sensitive to both pre-combustor temperature and regenerator effectiveness. Note that Risha et. al. predict that steam temperature and flow rate significantly affect flame stability [22]. Because the system geometry and the combustor performance are sensitive to pre-combustor temperature, even more care must be put into determining the operational temperature before finalizing the design.

Finally, this thesis has also demonstrated the flexibility of the NPSS architecture that allows the designer to concentrate on the physics of the problem by taking care of the 'details' associated with simulating complex multi-element systems. One major weakness of NPSS is that it is slow, especially when dealing with chemically reacting flows. Doing

the reacting flow calculations separately and using them to generate lookup tables can speed things up but implementing this technique is not at all obvious to the general NPSS user and requires a separate and significant time investment.

5.2   *Future Work*

Further work is required to determine how much lower the efficiency will fall in the low power delivery regime (if required). More work is also needed to model losses in the system, especially those in the connecting flow tubes. Additionally, a complete sensitivity analysis should be performed in order to understand which design parameters are the strongest determinants of performance so that engineering efforts can be focused on the most important design problems. The NPSS model can also be used to investigate the start up transient which has not yet been researched in any significant way. This study could also include investigating the ignition requirements for a ship-borne system. However, getting CEA to run 'in real time' would require significantly longer computational time.

Further work might also upgrade the model to include the complete system with models for hydrogen regeneration and the low temperature separator. Preliminary results from the model could be used to predict stable operating conditions and prescribe recirculation amounts and the required regenerator effectiveness. An upgraded model might include additional design parameters of interest.

Lastly, it is clear that any vehicle system can be optimized for one operating condition, however, the viability of the system may ultimately be determined, as in the case of scram-jets, by its off-design performance.   In the case of this Aluminum combustion-

based system, it remains to be proven that off-design performance of the combustor is possible at an acceptable or sustainable level.

Appendix (state points)

Open Cycle		Temperature	Pressure	Mass Flow	Quality	Enthalpy	Power	
Point	Description	°F	psia	lbm/sec	%	BTU/lbm	kW	Hp
1	Combustor Out							
2	Separator Power Steam Out							
3	Turbine Out							
4	Recuperator Hot Side Out							
5	Condenser Hot Side Out							
6	Feed Water Pump Out							
7	Recuperator Cold Side Out							
8	Combustor Water In							
9	Separator Regen Steam Out							
10	Steam Compressor In							
11	Steam Compressor Out							
13*	Aluminum							
14	Ambient Water							
	Condenser Cold Side Out							

Specific Fuel Consumption _____ lb/Hp-hr

Mechanical Power
Generator
Feedwater Pump
Steam Compressor
Water Intake Pump
Net

* Point 12, Fuel Feed Gas Supply not included in HS Analysis

Table taken from Ref. 39.

State	Description	Temperature (°F)	Pressure (psia)	Mass Flow (lb/sec)	Species
1	Combustor Outlet				
2	Turbine Inlet				
3	Turbine Exit				
4	Condenser Inlet				
5	Condenser Outlet				
6	Recuperator Water Inlet				
7	Recuperator Water Outlet				
8	Combustor Water Inlet				
9	Extracted Steam				
10	Tempered Extracted Steam				
11	Combustor Steam Feed				
12	Fuel Feed Gas Supply				
13	Fuel Feed				
14	Overboard				
V – Steam, H – Hydrogen, X – Alumina, L – Water, A – Aluminum					

Taken from Ref. 40.

Appendix (NPSS Code)

```
setThermoPackage("CEA","H2O","AL(cr)","H2O","H2O(L)","H2","AL2O3(a)","OH","H","ALOH" );
#include <InterpIncludes.ncp>
#include "Bleed.int";
#include "Separator.int";
#include "Seeder.int";
#include "H2OLoop.int";

real mass=xxxxx; // Run 2
Element H2Start F1{
        Pt = xxxx;
        Tt = xxxx;
        W = xxxx;}

Element Seeder Seed1{
        dPloss = xxxx;
        kSeed = xxxxx;
        void preexecute() {
//          cout<<"Seeder"<<endl;
        }
        }// End of Seeder

Element H2OLoop F2{ //first loop start
   Pt = xxxxx;
        Tt =xxxxx.;
        W = xxxxx;}


Element Bleed B1{ //pre-combustor element
        BleedInPort F1;
void preexecute(){
system( "copy thermo.lib org.lib" );
  system( "copy thermohot.lib thermo.lib" );   }

void postexecute(){
 system( "copy org.lib thermo.lib" );
   }
}

Element H2OStart F3{ //quench water start
        Pt = xxxxx;
        Tt = xxxxx.;
        W = xxxxx;          }

Element H2OLoop TurbOut{  //second loop start
        Pt = xxxxx;
        Tt = xxxxx;
        W = xxxxx }

Element HeatExchanger HE{ //Regenerator
        switchQcalc = "EFFECT";
        effect = xxxxx;
```

```
        dPqP1= xxxxx
        dPqP2= xxxxx;}

Element SplitterTT Split{
        BPR = xxxxx;}

Element Bleed B2{ //combustor
        BleedInPort F1;}

Element Separator Sep1{
        B= xxxxx;
        Ploss = xxxxx;
        effH2Sep = xxxxx;
        effH2OSep = xxxxx
        effAl2O3Sep = xxxxx;    }

Element Bleed B3{ //recirculation leg mixing
        BleedInPort F1;}

Element Compressor C1{
        switchMap = "EFF";
        eff = xxxxx;
        PRdes= xxxxx 3;}

Element Turbine T1{
        switchEff = "EFF";
        PRbase = xxxxx;
        eff = xxxxx;       }

Element Shaft Sh1{
        ShaftInputPort Turb , Comp1;
        HPX = xxxxx;}

Element FlowStart F4{ // ambient condenser water start
        Pt = xxxxx;
        Tt = xxxxx.;
        W = xxxxx;
        FuelStation Fu;

        void postexecute(){
          //quit();
          Fu.init( "H2O(L)", 0.,0.,0.,0.,0.,0.,0.,0.,0.,0. );
          Fu.Wfuel = xxxxx
          //Fu.Wfuel = xxxxx;
          //quit();
          Fl_O.burn( "Fu", 1.0 );
          //quit();
          Fl_O.setTotalTP( Tt, Pt );
          //quit();
        }
}

Element HeatExchanger Condenser{
        switchQcalc = "Q";
        //eff = xxxxx;
        Q = xxxxx;
```

```
        dPqP1= xxxxx;
        dPqP2= xxxxx;
}

Element FlowEnd E1;
Element FlowEnd AmbWarmed;
Element FlowEnd Eover;

//
//Seeder//
linkPorts( "F1.Fl_O", "Seed1.Fl_I", "start" );
linkPorts( "Seed1.Fl_O", "B1.Fl_I", "seed");

//Combustor//
linkPorts( "F2.Fl_O", "B1.F1", "recirc_end" );
linkPorts( "B1.Fl_O", "B2.Fl_I", "comb" );
linkPorts( "B2.Fl_O", "Sep1.Fl_I", "sep" );

//Quench water start//
linkPorts( "F3.Fl_O", "HE.Fl_I2", "HE_Cold_side");
linkPorts( "HE.Fl_O2", "Split.Fl_I", "quench_start");
linkPorts( "Split.Fl_01", "B2.F1", "quench_comb");
linkPorts( "Split.Fl_02", "B3.F1", "comb_in");
linkPorts( "B3.Fl_O", "C1.Fl_I", "comp1_start");
linkPorts( "C1.Fl_O", "F2.Fl_I", "comp1_end" );

//Separator//
linkPorts( "Sep1.Fl_O1R","B3.Fl_I","recirc_start");
linkPorts( "Sep1.Fl_O1T","T1.Fl_I", "turbine");
linkPorts( "Sep1.Fl_O2","Eover.Fl_I","over1");

// Separator with no turbine
//linkPorts( "Sep1.Fl_O1T","E1.Fl_I", "turbine");

//Recirculation//
//linkPorts( "F4.Fl_O", "B3.F1", "comb_in"); replaced by Quench water start
//compressor in recirc loop

// Turbine +HE hot side //
linkPorts( "T1.Sh_O", "Sh1.Turb" ,"Shaft");
linkPorts( "C1.Sh_O", "Sh1.Comp1", "compress");

//Heat Exchanger (Recuperator)
linkPorts( "T1.Fl_O", "TurbOut.Fl_I" , "Tout");
linkPorts( "TurbOut.Fl_O", "HE.Fl_I1" , "HE_hot_in");
linkPorts( "HE.Fl_O1", "Condenser.Fl_I1", "condense_in");
//Heat Exchanger (Condenser)
//linkPorts( "HEOut.Fl_O" , "Condenser.Fl_I1", "condense_in");
linkPorts( "F4.Fl_O", "Condenser.Fl_I2", "ambient_in");
linkPorts( "Condenser.Fl_O1", "E1.Fl_I", "condense_out");
linkPorts( "Condenser.Fl_O2", "AmbWarmed.Fl_I","ambient_out");

setOption( "switchInputSet", "SOLVED" );

//setOption( "switchDes", "OFFDESIGN");
autoSolverSetup();
```

105

```
solver.removeDependent( "Sh1.integrate_Nmech");
//take out the torque balance term"

Independent ByPass{
        varName = "Sep1.B"; }
Independent Squench{
        varName = "Split.BPR";}
Independent Effect{
        varName = "HE.effect";}
Independent FeedMass{
        varName = "F3.W";}

Dependent MassIn{
        eq_lhs = "C1.Fl_O.W";
        eq_rhs = "mass";}
Dependent RecircTemp{
        eq_lhs = "C1.Fl_O.Tt";
        eq_rhs = " xxxxx ";}
Dependent RecoopTemp{
        eq_lhs = "HE.Fl_O2.Tt";
        eq_rhs = " xxxxx ";}

Dependent constraint_MinB {
   eq_lhs = "Sep1.B";
   eq_rhs= " xxxxx ";}

Dependent constraint_MaxB {
   eq_lhs = "Sep1.B";
   eq_rhs= " xxxxx ";}

MassIn.addConstraint("constraint_MinB","MIN");
MassIn.addConstraint("constraint_MaxB","MAX");

solver.addIndependent( "ByPass" );
solver.addDependent( "MassIn" );
solver.addIndependent( "Squench");
solver.addDependent( "RecircTemp");
solver.addIndependent( "Effect");
solver.addDependent( "RecoopTemp");
cout << "\n\nDesign Dependents:\n" << solver.dependentNames;
cout << "\n\nDesign Indepenents:\n" << solver.independentNames;

setOption("switchTransport","EQUIL"); //set chemistry to equilibrium

run(); //runs the model
```

Bibliography

1. **Miller, Timothy F., Walter, Jeremy L. and Kiely, Daniel H.** *A Next Generation AUV Energy System Based on Aluminum-Seawater Combustion.* State College, PA : Applied Research Lab, 2003.

2. **Hill, P.G. and Peterson, C.R.,** *Mechanics and Thermodynamics of Propulsion*, Reading, MA: Addison-Wesley Publishing Company, 1965.

3. **Snyder, Paul E. and Harry, Seltz.** *Heat of Formation of Aluminum Oxide.* s.l. : Carnegie Institute of Technology Department of Chemistry, 1945.

4. *Estimating aluminium particle combustion kinetics .* **Bartlett, R. W., et al.** s.l. : Combustion and Flame, 1963, Vol. 7. Pages 227-234.

5. *Aluminum Particle Combustion.* s.l. : Defense Technical Information Center, April 1966. NOTS-TP-3916.

6. *Ignition and combustion of aluminium particles in hot ambient gases.* **Friedman, R. and Macek, A.** s.l. : Combustion and Flame, 1962, Vol. 6. Pages 9-19..

7. *The ignition and combustion of aluminum and beryllium (Metal ignition and combustion of aluminum and beryllium).* **Kuehl, D. K.** New York, NY : 2nd AIAA Aerospace Sciences Meeting and Exhibition, Jan 1965.

8. **Gordon and McBride.** *Chemical Equilibirum with Applications (CEA2).* [Software] s.l. : NASA Glenn Research Center, 2002. NASA RP-1311.

9. *Experimental investigation of aluminum particle dust cloud combustion.* **Risha, Grant A., et al.** Reno, NV : 43rd AIAA Aerospace Sciences Meeting and Exhibit, January 2005. AIAA 2005-739.

10. *Quenching Distance of Laminar Flame in Aluminum Dust Clouds.* **Goroshin, S., Bidabadi, M. and Lee, J.H.S.** 1-2, s.l. : Combustion and Flame, April 1996, Vol. 105. Pages 147-160.

11. *Experimental study of aluminum particle flame evolution in normal and micro-gravity.* **Dreizin, Edward L.** 3, s.l. : Combustion and Flame, June 1999, Vol. 116. Pages 323-333.

12. *Condensed-phase species distributions about Al particles reacting in various oxidizers.* **Bucher, P., et al.** 1-2, s.l. : Combustion and Flame, April 1999, Vol. 117. Pages 351-361.

13. *Ignition and combustion of aluminum in oxygen/nitrogen mixture streams.* **Yuasa, Saburo, Zhu, Yuxiu and Sogo, Sakurako.** 4, s.l. : Combustion and Flame, March 1997, Vol. 108. Pages 387-390.

14. *Experimental study of stages in aluminium particle combustion in air.* **Dreizin, Edward L.** 4, s.l. : Combustion and Flame, June 1996, Vol. 105. Pages 541-556.

15. *Flame propagation in bimodal nano/micro-sized aluminum particle/Air mixtures.* **Huang, Ying, et al.** Reno, NV : 44th AIAA Aerospace Sciences Meeting and Exhibit, January 2006. AIAA 2006-1155.

16. *Aluminum combustion in wet and dry CO2: Consequences for surface reactions.* **Sarou-Kanian, V., et al.** 1-2, s.l. : Combustion and Flame, April 2006, Vol. 145. Pages 220-230.

17. *Aluminum combustion modeling in solid propellant environments.* **Widener, J. F., Liang, Y. and Beckstead, M. W.** Los Angeles, CA : 35th AIAA/ASME/SAE/ASEE Joint Propulsion Conference and Exhibit, June 1999. AIAA 1999-2629.

18. *Model of Aluminum Agglomerate Evolution in Combustion Products of Solid Rocket Propellant.* **Babuk, V.A. and Vasilyev, V.A.** 4, s.l. : AIAA Journal of Propulsion and Power, August 2002, Vol. 18. Pages 814-823.

19. *Energetics of Aluminum Combustion.* **Politzer, Peter, Lane, Pat and Grice, M. Edward.** A, s.l. : Journal of Physical Chemistry, May 2001, Vol. 105. Pages 7473-7480.

20. *Dynamics of Aluminum Combustion.* **Brooks, Kristen P. and Beckstead, Merrill W.** 4, s.l. : AIAA Journal of Proplulsion and Power, August 1995, Vol. 11. Pages 769-780.

21. *Surface phenomena in aluminum combustion.* **Trunov, Michael A. and Dreizin, Edward L.** 3, s.l. : Combustion and Flame, May 1995, Vol. 101. Pages 378-382.

22. *Combustion of Aluminum Particles with Steam and Liquid Water.* **Risha, Grant A., et al.** Reno, NV : 44th AIAA Aerospace Sciences Meeting and Exhibit, 2006. AIAA 2006-1154.

23. *Shock tube measurements of combustion of nano aluminum.* **Bazyn, Tim, Krier, Herman and Glumac, Nick.** Reno, NV : 44th AIAA Aerospace Sciences Meeting and Exhibit, January 2006. AIAA 2006-1157.

24. *Analysis of Nano-Aluminum Particle Dust Cloud Combustion in Different Oxidizer Environments.* **Huang, Ying, et al.** Reno, NV : 43rd AIAA Aerospace Sciences Meeting and Exhibition, January 2005. AIAA 2005-738.

25. *The mechanism of combustion of superfine aluminum powders.* **Kwon, Young-Soon, et al.** 4, s.l. : Combustion and Flame, June 2005, Vol. 133. Pages 385-391.

26. *Combustion of Nano-Aluminum and Liquid Water.* **Risha, G. A., et al.** 2, s.l. : Proceedings of the Combustion Institute, January 2007, Vol. 31. Pages 2029-2036..

27. *The effects of aluminum size on the combustion characteristics of high energy propellants with higher burning rates.* **Li, S.F., et al.** Sacremento, CA : 42nd AIAA/ASME/SAE/ASEE Joint Propulsion Conference and Exhibit, July 2006. AIAA 2006-4930.

28. *Investigation of Aluminum Particle Combustion for Underwater Propulsion Applications.* **Foote, John P., et al.** Buena Vista, FL : 32nd AIAA/ASME/SAE/ASEE Joint Propulsion Confernce and Exhibit, 1996. AIAA 1996-3086.

29. **Greiner, Leonard.** *Underwater Misslie Propulsion.* Arlington, VA : Compass Publications, Inc., 1967.

30. *Fluidized Powders-A New Approach to Storable Missle Fuels.* **Fricke, H.D., Burr, J.W. and Sobieniak, M.G.** 12th JANNAF Liquid Propulsion Meeting : CPIA Publication, 1970. 201.

31. *Comments on "Role of Aluminum in Suppressing Instability in Solid Propellant Rocket Motors".* **Price, E.W.** 5, s.l. : AIAA Journal, May 1971, Vol. 9. Pages 987-990.

32. *Green rocket propulsion by reaction of Al and Mg Powders and Water.* **Miller, Timothy F. and Herr, John D.** Fort Lauderdale, FL : AIAA/ASME/SAE/ASEE Joint Propulsion Conference and Exhibit, July 2004. AIAA 2004-4037.

33. *Aluminum for Space Propulsion.* **Ingenito, Antonella and Bruno, Claudio.** 4, s.l. : AIAA Journal of Propulsion and Power, December 2004, Vol. 20. Pages 1056-1063.

34. *Thermochemistry of aluminum species for combustion modeling from Ab Initio molecular orbital calculations.* **Swihart, Mark T. and Catoire, Laurent.** 1-2, s.l. : Combustion and Flame, April 2000, Vol. 121. Pages 210-222.

35. *Steady metal combustor as a closed thermal energy source.* **Groff, E.G. and Faeth, G.M.** s.l. : Journal of Hydronautics, 1978, Vol. 12. Pages 63-70.

36. **Kiely, Daniel H.** *Review of Underwater Thermal Propulsion.* s.l. : AIAA, 1994. AIAA-94-2837.

37. **Nasa Glenn Research Center.** *Numerical Propulsion System Simulation.* [Software in Unix, Windows, and Linux] s.l. : Wolverine Ventures, Inc., 2003.

38. *Optimization of Coupled Systems: A Critical Overview of Approaches* **Balling R.J. and Sobieszczanski J.** 1-2 s.l. : January 1996 AIAA Journal Vol. 34. Pages 6-17.

39. **Hamilton Sunstrand.** Aluminum Combustor Systems Analysis Open vs Closed Cycle. *E-mail Correspondence with Joe Fontaine.* 2006.

40. **Herr, J. et. al.** *StatusHighlights.pdf.* [E-mail] 2006.

41. **Wolverine Ventures Inc.** NPSS Users Guide (permission required to download). [Online] 2002. www.virtualtestcell.com.

42. —. NPSS Developers Guide (permissions required to download). [Online] 2002. www.virtualtestcell.com.

43. **Brennen, C.** *Fundamentals of Multiphase Flow.* New York : Cambridge University Press, 2005.

44. **Cengel, Y and Boles, M.** *Thermodynamics: An Engineering Approach 4th ed.* New York : McGraw Hill, 2002.